LAPPEENRANTA UNIVERSITY OF TECHNOLOGY

School of Technology

LUT Energy, Electrical Engineering

Sergei Kryltcov

DOUBLY FED WIND TURBINE PERFORMANCE IN VARIABLE GRID CONDITIONS

Lappeenranta

Examiners: Professor Olli Pyrhönen

Professor Pasi Peltoniemi

ABSTRACT

Lappeenranta University of Technology
School of Technology
LUT Energy, Electrical Engineering

Sergei Kryltcov

Doubly fed wind turbine performance in variable grid conditions

Master's Thesis
2015
90 pages, 35 pictures, 3 tables.
Examiners: Professor Olli Pyrhönen and Professor Pasi Peltoniemi

Keywords: DFIG, wind turbine, vector control, reactive power control, power analysis.

Wind turbines based on doubly fed induction generators (DFIG) become the most popular solution in high power wind generation industry. While this topology provides great performance with the reduced power rating of power converter, it has more complicated structure in comparison with full-rated topologies, and therefore leads to complexity of control algorithms and electromechanical processes in the system.

The purpose of presented study is to present a proper vector control scheme for the DFIG and overall control for the WT to investigate its behavior at different wind speeds and in different grid voltage conditions: voltage sags, magnitude and frequency variations. The key principles of variable-speed wind turbine were implemented in simulation model and demonstrated during the study. Then, based on developed control scheme and mathematical model, the set of simulation is made to analyze reactive power capabilities of the DFIG wind turbine. Further, the rating of rotor-side converter is modified to not only generate active rated active power, but also to fulfill Grid Codes. Results of modelling and analyzing of the DFIG WT behavior under different speeds and different voltage conditions are presented in the work.

ACKNOWLEDGEMENTS

I would like to express my sincere gratitude to my supervisors, Professor Olli Pyrhönen, Professor Pasi Peltoniemi and Doctoral Student Elvira Baygildina for their continuous support, guidance, invaluable help and friendly atmosphere during the study.

I would like to express special thanks to my family and friends for their support and patience.

Contents

NOMENCLATURE

Symbols

$\bar{i}_f$ – current vector across the capacitor in LCL-filter

$\bar{i}_g$ – grid current vector

$\bar{i}_i$ – GSC current vector

$\bar{i}_r$ – rotor current vector

$\bar{i}_s$ – stator current vector

$\overline{v}_f$ – LCL-filter voltage vector

$\overline{v}_g$ – grid voltage vector

$\overline{v}_i$ – GSC voltage vector

$\overline{v}_r$ – rotor voltage vector

$\overline{v}_s$ – stator voltage vector

$\overline{\psi}_r$ – rotor flux

$\overline{\psi}_s$ – stator flux vector

ω_r – rotor rotational speed

A_r – area swept by WT rotor

B_{hgb} – damping coefficient between hub and gearbox

B_{bh} – damping coefficient between blades and hub

B_{gbg} – damping coefficient between gearbox and generator

C_{dc} – DC-link capacitance

C_f – LCL-filter capacitance

C_p – power coefficient

D_h – hub friction coefficient

D_G – generator friction coefficient

D_{GB} – gearbox friction coefficient

D_b – blades friction coefficient

E_d – back EMF direct component

E_{dc} – DC-link stored energy

E_k – kinetic energy of the moving air mass

E_q – back EMF quadrature component

J_h – hub inertia

J_G – generator's rotor inertia

J_{GB} – gearbox inertia

J_b – blade inertia

L_{f1} – GSC-side filter inductance

L_{f2} – grid-side filter inductance

L_m – mutual inductance

$L_{\sigma r}$ – rotor leakage inductance

$L_{\sigma s}$ – stator leakage inductance

P_{dc} – DC-link active power

P_f – active power on LCL-filter

P_i – active power at GSC-side

P_{m_rated} – mechanical power produced on low-speed shaft at nominal wind speed

P_{mec} – actually captured mechanical power

P_{out} – active power delivered to the grid

P_w – full power theoretically available for capturing from the wind

Q_i – reactive power at GSC-side

Q_s – stator instantaneous reactive power

R_c – DC-link shunt resistance

R_f – LCL-filter equivalent resistance

R_{f1} – GSC-side filter resistance

R_{f2} – grid-side filter resistance

R_{f3} – capacitor circuit filter resistance

R_r – rotor resistance

R_s – stator resistance

T_e – electromagnetic torque produced by IG

T_m – mechanical torque at the IG shaft input

T_{w_rated} – torque applied to the WT blades at nominal wind speed

V_{grid} – grid voltage magnitude

X_f – LCL-filter equivalent reactance

Z_f – LCL-filter equivalent impedance

f_g – grid voltage frequency

i_{dc} – DC-link current

i_f – current across capacitor in LCL-filter

i_{fd} – LCL-filter current direct component

i_{fq} – LCL-filter current quadrature component

i_g – grid current

i_i – GSC current

$i_{rated\ d}$ – rated current direct component of power converter

$i_{rated\ q}$ – rated current quadrature component of power converter

i_{rated} – rated current magnitude of power converter

i_{rd} – rotor current direct component

i_{rq} – rotor current quadrature component

i_{sd} – stator current direct component

i_{sq} – stator current quadrature component

k_{hgb} – stiffness between hub and gearbox

k_I – integral gain of PI-regulator

k_P – proportional gain of PI-regulator

k_{PI} – function of PI-regulator

k_{bh} – stiffness between blades and hub

k_{dt} – drivetrain gear ratio

k_{gbg} – stiffness between gearbox and generator

n_r – number of rotor windings turns

n_s – number of stator windings turns

q_{dc} – DC-link capacitor charge

r_r – rotor radius

s_a – switching function of the top (positive DC-link terminal) switch in phase A of power converter

s'_a – switching function of the bottom (negative DC-link terminal) switch in phase A of power converter

s_b – switching function of the top (positive DC-link terminal) switch in phase B of power converter

s_b' – switching function of the bottom (negative DC-link terminal) switch in phase B of power converter

s_c – switching function of the top (positive DC-link terminal) switch in phase C of power converter

s_c' – switching function of the bottom (negative DC-link terminal) switch in phase C of power converter

v_{sa} – voltage at the phase A terminal of the power converter

v_{sb} – voltage at the phase B terminal of the power converter

v_{sc} – voltage at the phase C terminal of the power converter

v_{dc} – DC-link voltage

v_g – grid voltage

v_i – GSC applied voltage

v_{rd} – rotor voltage direct component

v_{rq} – rotor voltage quadrature component

v_{sd} – stator voltage direct component

v_{sq} – stator voltage quadrature component

v_w – wind speed

$\overline{x}$ – arbitrary vector

x_a – phase A component of arbitrary parameter in three-phase stationary reference frame

x_b – phase B component of arbitrary parameter in three-phase stationary reference frame

x_c – phase C component of arbitrary parameter in three-phase stationary reference frame

x_d – direct-axis arbitrary component in synchronous rotational frame

x_q – quadrature-axis arbitrary component in synchronous rotational frame

x_α – alpha-axis component of arbitrary parameter in two-phase stationary reference frame

x_β – beta-axis component of arbitrary parameter in two-phase stationary reference frame

x_γ – gamma-axis component of arbitrary parameter in two-phase stationary reference frame

θ_0 – initial displacement of arbitrary vector

θ_h – hub angular displacement

θ_G – generator rotor angular displacement

θ_b – blade mass angular displacement

λ_{opt} – optimal tip speed ratio

ψ_{rd} – rotor flux direct component

ψ_{rq} – rotor flux quadrature component

ψ_{sd} – stator flux direct component

ψ_{sq} – stator flux quadrature component

ω_h – hub rotational speed

ω_b – WT rotor blade rotational speed

ω_{dq} – angular frequency of synchronous rotational frame

ω_g – rotational speed of grid voltage vector

ω_r – generator's rotor rotational speed

ω_{r_max} – maximum allowed rotor speed

ω_s – rotational speed of stator magnetic field

S – stator instantaneous apparent power

m – air mass

p – number of IG pole pairs

s – slip

t – time parameter

β – WT blades pitch angle

θ – angular displacement of arbitrary vector

λ – tip speed ratio

ρ – air density

ϕ – angular displacement between grid voltage and current vector

Abbreviations

AC – alternating current

DC – direct current

DFIG – doubly-fed induction generator

DPC – direct power control

DTC – direct torque control

EMF – electro motive force

FOC – field oriented control

GSC – grid-side converter

IG – induction generator

IGBT – insulated-gate bipolar transistor

IM – induction machine

PCC – point of common coupling

PI – proportional/integral (regulator)

PLL – phase locked loop

PWM – pulse width modulation

RSC – rotor-side converter

SFO – stator flux oriented (frame)

SRF – synchronous reference frame

SVM – space vector modulation

TSR – tip speed ratio

VOC – voltage oriented control

WT – wind turbine

1 INTRODUCTION

1.1 Backgrounds

According to "Renewable Energy Directive" of the European Parliament and of the Council issued on 17.10.2012 (Renewable Energy Directive, 2012) the share of renewable energy sources in overall European power generation should increase to 20% by 2020. The directive claims the subsidiarity policies for generation companies and stimulates developing of both renewable energy capacities and technologies.

Wind power is one of the major components of renewable energy generation. In Finland today the wind power generation shares about 1 percent of total power generation and is continuously increasing. Only for the last five years Finnish wind power-generating capacities have increased more than three times – from 160 to 520 MW. The growth of wind power generation capacities and productivity in Finland for the last five years is shown in the Figure 1.1.

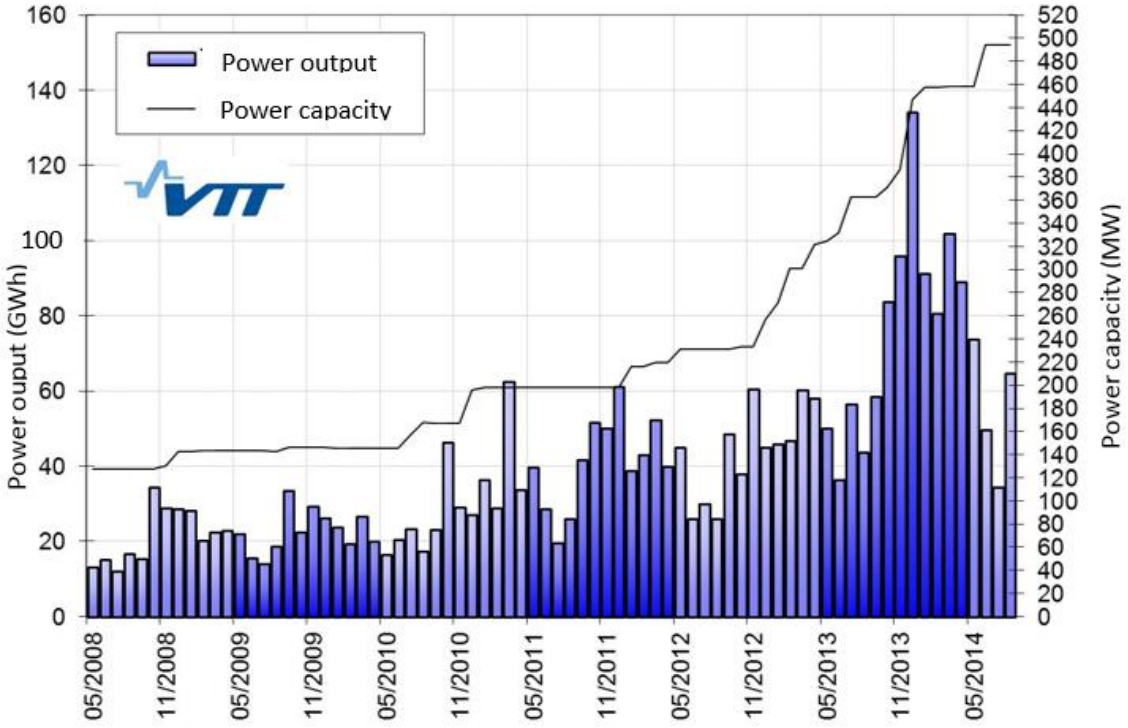

Figure 1.1. Growth of wind power-generating capacity and productivity in Finland for the last 5 years. (VTT, n.d.)

The exponential growth of the wind power capacities is also fair for worldwide wind power generation. In 2012, for example, both China and the United States surpassed 50,000 MW capacities of all wind turbines and wind farms connected to the grid across the countries.

Another important tendency is continuously increasing average power ratings and overall size of single wind turbines. The situation is illustrated in Figure 1.2. The average rated capacity of new grid-connected onshore turbines in 2012 was 1.8 MW, compared to 1.6 MW in 2008, though the largest commercial wind turbine available today is 7.5 MW, with a rotor diameter of 127 meters. Offshore turbine sizes have grown from 3 MW to 4 MW in 2012. However, turbines with a rated capacity ranging from 1.5 MW to 2.5 MW still make up the largest market segment. (Arapogianni & Genachte, 2013) Increased size of wind turbines is also closely related to continuously increasing power ratings of electrical drives and power electronics equipment.

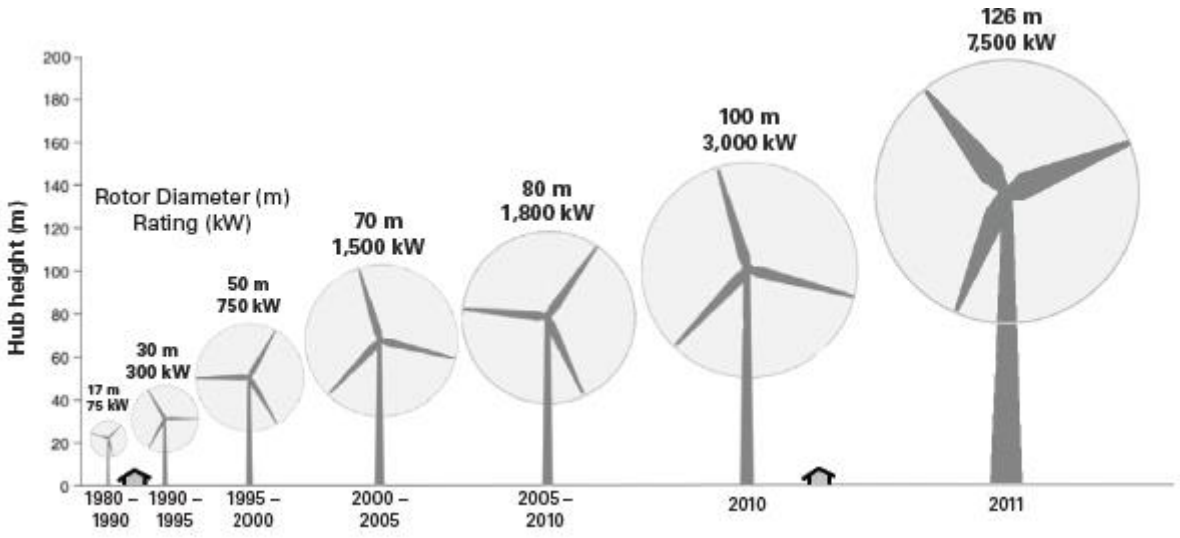

Figure 1.2. Tendency to increase in power ratings and size of wind turbines. (Patel, 2013)

Described tendencies become the main drivers for both electricity market and power equipment manufacturers. Growth of wind power generation industry leads to increased demands to power quality produced by the WTs, which are considered in the latest Grid Codes (for Finland and some other countries). The primary goal of WT manufacturers then becomes the producing of cost-effective WT solution, which at the same time is able to provide necessary power quality.

1.2 Wind turbine concepts

There are two concepts of WTs – horizontal axis WT and vertical axis WT. While vertical axis WT have much lower efficiency than horizontal-axis, their use in multi-megawatt wind power industry is very limited (Burton, Jenkins, Sharpe, & Bossanyi, 2011). Therefore, only horizontal-axis WT are considered in the presented study.

All WT are divided in separate groups by type of generator used and type of its connection to the grid. Among the variety of available WT solutions all horizontal-axis WTs can be mainly divided in two groups by operation principle: fixed-speed WTs, where there is no control of WT rotor speed; and variable-speed WTs, rotor speed of which is controlled in definite range.

1.2.1 Fixed-speed wind turbines

First industrial wind turbines were built according to Danish concept. Design of this easiest concept is illustrated in Figure 1.3 and usually called fixed-speed wind turbines, because there is no availability to control the rotor speed. Fixed-speed wind turbine consists of induction generator (IG) with squirrel-caged rotor, which is connected directly to the grid. IG absorbs reactive power from the grid and therefore fixed-speed WT is usually combined with the capacitor bank, which compensates reactive power. Starting currents of IG exceed nominal more than a few times and for current limitation purpose soft starters are usually required.

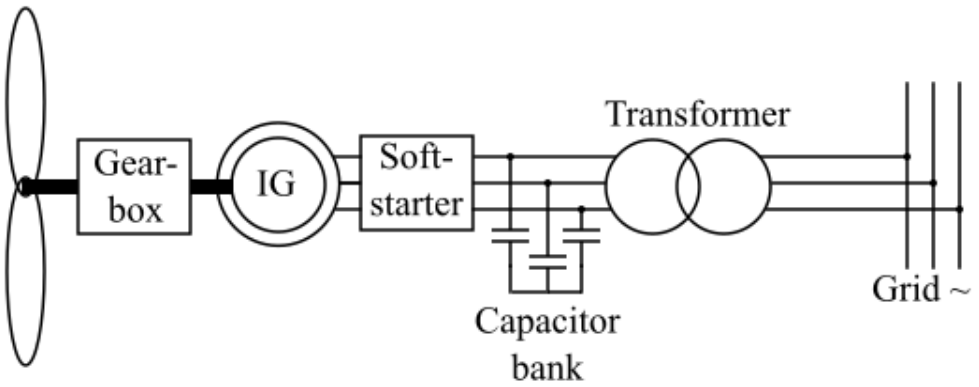

Figure 1.3. Fixed-speed wind turbine concept (“Danish concept”). (Petersson A. , 2005)

According to fixed-speed WT design, rotor speed is bound to the grid voltage frequency and therefore every fluctuation of wind torque applied to the blades will lead to fluctuations of output power generated by the wind turbine. These power fluctuations is the one important disadvantage of fixed-speed wind turbines, which means poorer generated power quality and higher stresses in mechanical parts of wind turbine. Another one drawback is WT catches different amount of power from the wind depending on both the wind velocity and the IG rotor speed, so if it is impossible to control rotor speed – WT will not catch the maximum possible power.

Gearbox is optional component, which is required to adapt rotor speed to the grid frequency, because of very low speed of the WT shaft with blades. Another way to increase rotor speed is to increase the number of poles in generator, so the drivetrain is not required. Danish concept has next characteristics:

- The simplest design – does not require any power converters.
- Non-maximal power extraction.
- High mechanical and electrical stresses.
- Requires soft-starter and capacitor bank.

1.2.2 Variable-speed WT with full rated converter

Huge development of power electronics from 1980-s led to becoming of power converters a de-facto standard in many industrial applications and branches including wind power generation industry. Use of power converters in the wind turbine allowed to eliminate main disadvantages of fixed-speed wind turbines.

Variable-speed wind turbine design is presented in the Figure 1.4. According to this topology, the generator, which can be IG with squirrel-caged rotor or the synchronous generator on permanent magnets (PMSG), is connected to the grid via the full-rated back-to-back power converter.

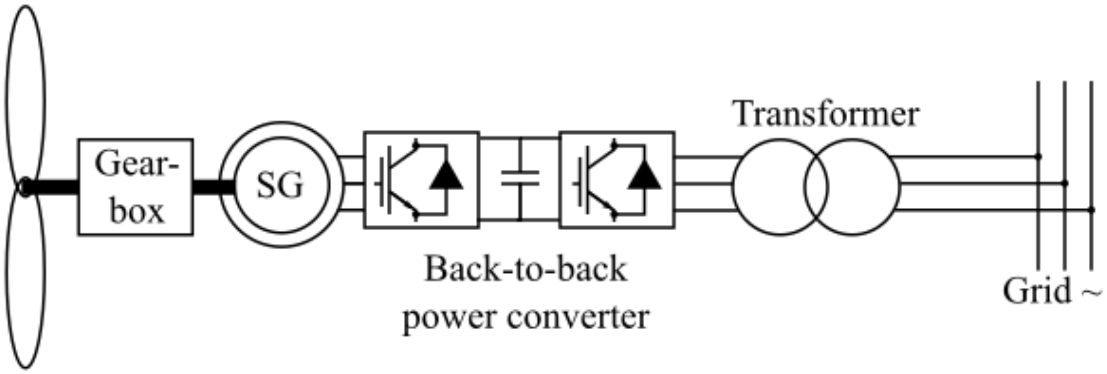

Figure 1.4. Variable-speed wind turbine with full-rated power converter. (Petersson A. , 2005)

Use of the back-to-back power converter allows decoupling of grid and generator. That means that generator-side inverter controls rotor speed and generated power while grid-side inverter controls the exchange of reactive and active power between the grid and DC-link. Therefore, DC-link acts as power "buffer" here. Full rated converter WT topology has next benefits:

- Control of rotor speed. That means:
  - Reduced mechanical and electrical stresses, because power variations smooth by rotor speed control and storage of power in DC-link capacitor.
  - Extraction of maximum power by rotor speed control.
- Independent control of active and reactive power exchange between the WT and grid.
- Electrical efficiency highly depends on power converter efficiency.

1.2.2 Doubly-fed induction generator wind turbines

While use of power converters for connection of generators to the grid has become a quite cost-effective solution in wind power industry, it also brings drawbacks of power electronics in WT design – power equipment has relatively high price especially for high power rated applications and it also provides losses in power circuits.

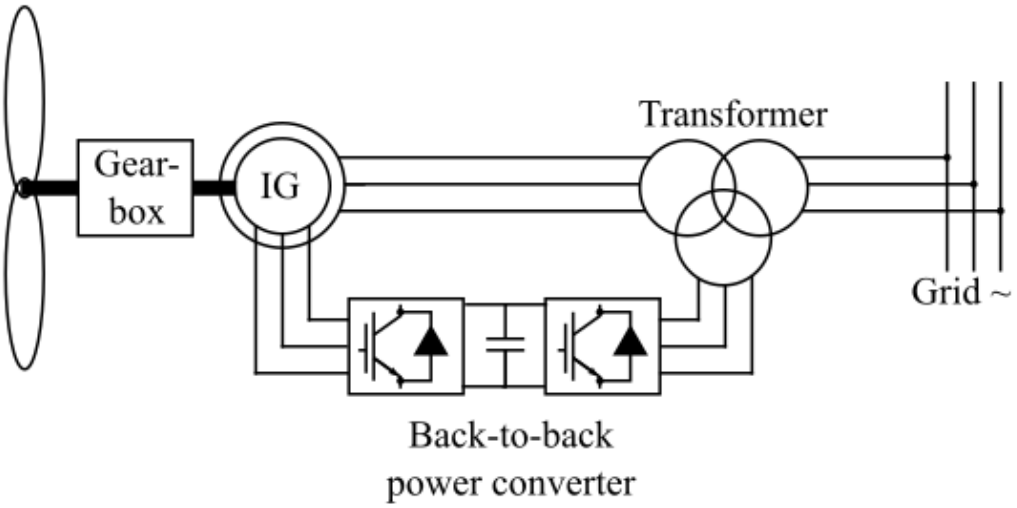

Figure 1.5. Variable-speed WT – DFIG topology. (Petersson A. , 2005)

DFIG concept (Figure 1.5) has appeared as a result of dealing with disadvantages of variable-speed wind turbines with full-rated converter (Fletcher & Yang, 2010). This concept uses induction generator with wound rotor, which has both stator and rotor three-phase windings. Stator is connected directly to the grid, while rotor is connected to the grid via the back-to-back power converter and slip rings. DFIG wind turbine is usually connected to the grid via three-winding transformer. In the DFIG topology only small part (about 25%) of whole power flows through the rotor circuit that leads to the key advantage of such concept – back-to-back converter in the rotor circuit is rated only to one third of whole wind turbine power rating.

Reduced power rating of converter means lower prices and sizes of all devices included in rotor circuit – IGBT inverters, DC-link capacitor, grid filters in comparison with the same devices in full-rated back-to-back converter. This also means lower magnetizing and thermal losses in power equipment and less dependency of wind turbine performance on the converter efficiency.

- Reduced to 25-30% power rating of back-to-back power converter in comparison with full rated converter WT design. That means:
    - Lower costs of power electronics equipment.
    - Lower magnetizing and thermal losses.
    - Lower but still suitable rotor speed operating range.
- Higher maintenance costs because of slip rings and brushes in the IG.

1.3 Objectives of the thesis

Adequate model. DFIG WT is a complicated system and its performance investigation requires a model, which on the one hand adequately represents real dynamical physical processes involved in power generation and on the other hand allows to simulate the system on the large time ranges, as some of the process require some time to be investigated. Therefore, it raises an issue of deciding which parts should be modelled in every detail and which processes can be approximated on the basic level.

Control system. Placing power converter in the rotor circuit requires sophisticated control algorithms, which should provide decoupled control of active and reactive power produced at stator terminals by maintaining rotor currents.

Power flows and performance analysis. Separate rotor and stator circuits lead to existence of two sources/consumers of reactive and active power in the WT circuit. It provides behavior that is more complex for power generation and requires additional analysis. At the same time, as a variable-speed topology DFIG WT control system should adequately extract maximum available power from the wind. It also states some design challenges such as choice of power converter power rating, as it mostly defines variable-speed range as well as reactive power capabilities of the DFIG WT.

Reactive power capabilities. As both DFIG and grid-side inverter can be used to control reactive power, it is essential to analyze limitations of the DFIG WT depending on different wind speeds and different grid conditions.

Grid codes fulfillment. As any generation power plant, DFIG WT should fulfill so-called grid codes – global requirements for power quality and capabilities of and energy source connected to the grid. Grid codes state many factors, which WT should fulfill, among which are the voltage sag ride-through ability, power factor correction requirements, and voltage variations ride-through.

Therefore, the thesis is devoted to detailed investigation of the DFIG WT behavior in different wind speeds and grid conditions, which can be divided in two major parts. First is the

investigation of active power generation, capabilities and limitations under different wind conditions. Second part considers capabilities of reactive power generation and limitations of the DFIG WT as well as its performance under grid voltage disturbances.

1.4 Thesis structure

According to described challenges of the DFIG WT topology through the thesis there were solved several objectives and thesis is organized according to these objectives into five chapters:

1. Chapter 1, the Introduction, provides backgrounds of modern wind power generation. It indicates recent trends in wind power industry. Then available WT topologies are presented and their advantages and disadvantages are indicated. Based on backgrounds, the motivation of research is presented. Chapter 1 also contains the scope and structure of the thesis.

2. Chapter 2, the DFIG WT modeling, presents mathematical description of the most important processes involved in power conversion process of the DFIG WT as well as its implementation in the PLECS simulation toolbox. Firstly, the considered DFIG WT electromechanical system is presented, from which the main domains are selected. Further mathematical representation and model implementation of each domain is discussed with the focus on electrical domain.

3. Chapter 3, the Control of DFIG WT, presents the derivation of algorithms, utilized by vector control system of the back-to-back power converter. The Chapter 3 focuses on presenting of basic control laws in the time domain and it does not consider tuning of PID regulators, anti-windup techniques, et cetera.

4. Chapter 4, the Operation of DFIG WT, contains implementation and verification of the DFIG WT principles on the simulation model. The chapter considers active power flows in steady-state operation, implementation of pitch angle control. As final step – the operating regions of the DFIG WT are indicated and then model is tested in dynamic

conditions – wind speed variations. The power converter rating is chosen to provide rated amount of power to the grid.

5. Chapter 5, the Reactive power control of DFIG WT, presents set of simulations, which illustrate natural reactive power flow in the DFIG WT circuits, reactive power capabilities at different wind speeds, and fulfilling Grid Codes: adapting of power converter rating for providing necessary power factor in undervoltage and overvoltage conditions, surviving voltage sags and grid voltage control.

2 DFIG WT model

This chapter contains information about DFIG WT principles of operation, components, mathematical model and its implementation in simulation software. The overall view of DFIG WT system is presented in the first part of the chapter, and then different stages of power conversion process as well as corresponding system components are indicated. Later each component and principle of implementation in computational model is discussed.

2.1 DFIG WT system overview

WT system converts energy contained in the wind into electrical power, which is then being delivered to the grid. The power conversion process takes place in several stages.

1. The power contained in the wind gusts is caught by WT rotor blades and transformed into rotational movement of the WT shaft.
2. Low-speed WT shaft rotational movement is transformed to the high-speed generator shaft by use of gearbox.
3. Mechanical rotation of the generator rotor induces rotational electromagnetic field and electrical power produced on the stator side.
4. Generated power is converted and delivered in a suitable way for the consumer demands.

Each stage of power conversion produces a noticeable effect on the total power generation and therefore adequate model of each stage of the conversion process is required for study purposes. Similarly, DFIG WT model can be also divided into several domains according to the nature of physical processes involved:

- Aerodynamic model
- Mechanical model
- Power circuit model

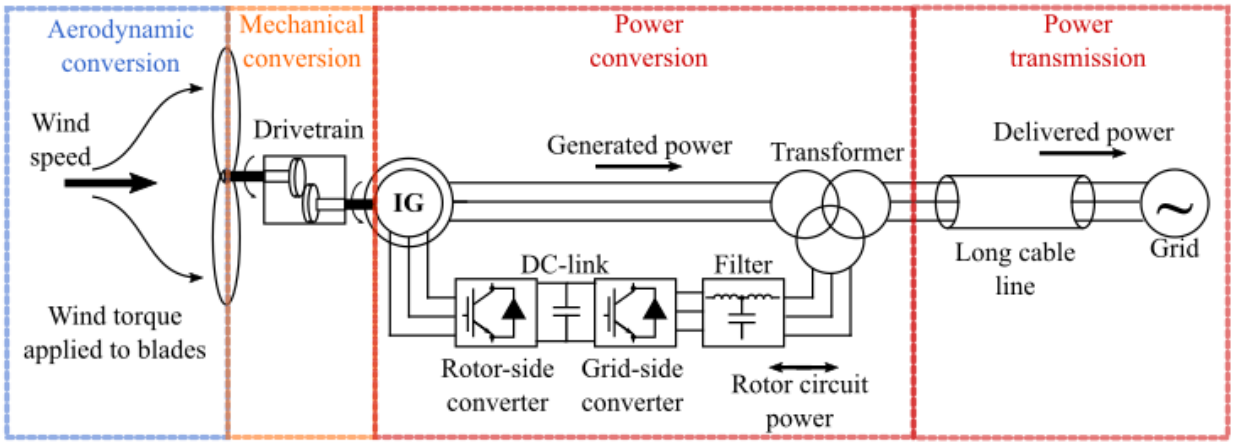

Figure 2.1. The DFIG WT electromechanical system

DFIG WT electromechanical system is presented in Figure 2.1. According to it, power generation goes through different stages. WT model should adequately simulate these stages by corresponding sets of equations and other representation data, such as look up tables, et cetera. Power generation process starts from the aerodynamic conversion process, in which wind gust torque is being applied to the WT blades. In such situation, WT blades extract some part of power contained in the moving air mass and transfer it to rotational movement of the WT low-speed shaft. As IG requires much higher rotational speed (~1500–3000 RPM) than can be possibly achieved by low-speed shaft (10-20 RPM), the gearbox transfers low-speed rotation to the high-speed rotation. That stage represents mechanical conversion process. High-speed shaft is connected directly to the IG rotor, where high-speed rotational movement used to generate a rotational magnetic field induced by the rotor windings. Magnetic field couples with stator windings and produces current flow and therefore generates power that is being delivered to the grid. However, as rotor windings are also connected to the grid via power converter, there is some power circulating in the rotor circuit. Both stator and rotor circuits are connected to the transmission line via three-winding transformer, forming point of common coupling (PCC), and then power has been transferred to the customer or grid through long cable line.

2.2 Implementation in the PLECS simulation toolbox

Model implementation is carried out in the PLECS simulation toolbox. PLECS (Piecewise Linear Electrical Circuit Simulation) is a toolbox for Simulink produced by Plexim GmbH and designed especially for power electrical circuits simulations. PLECS library contains built-in

DFIG WT detailed model, which was taken as a basis for study. However, initially the model was intended to demonstrate only basic principles of the DFIG WT operation and is not suitable enough for purposes of study. Hence, some modifications are applied to the model and are described in this and next chapters.

PLECS simulation toolbox includes built-in objects from different domains and allows its interconnection, which is the key advantage of this software. For example, there are mechanical circuits, electrical circuits, thermal and magnetic models, which makes PLECS the suitable environment for the DFIG WT detailed simulation.

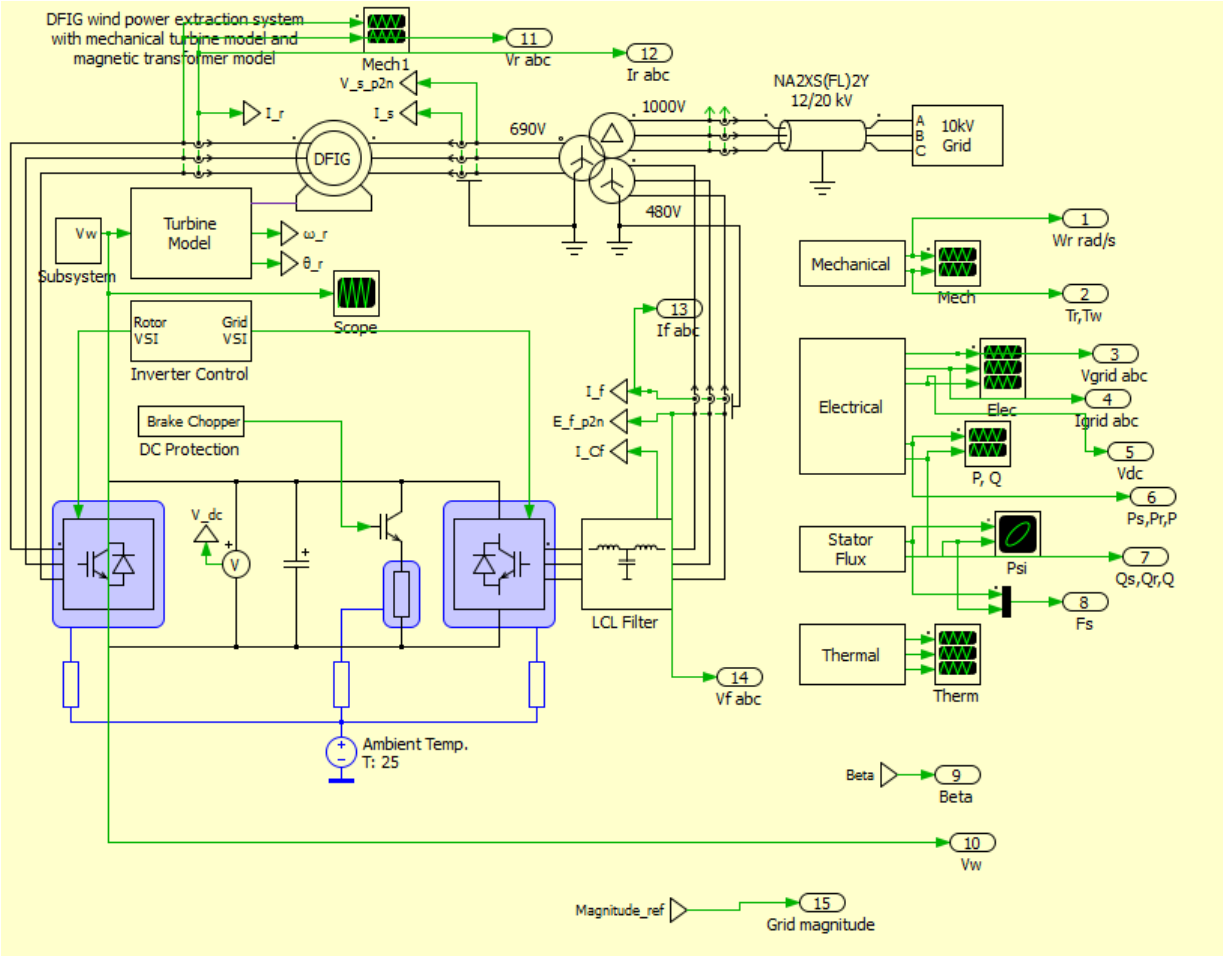

Figure 2.2. The DFIG WT PLECS model.

DFIG WT model structure implemented in PLECS library is shown in the Figure 2.2. The model will be described in details through this chapter, but now it can be seen that model contains:

2.2 Aerodynamic model

The aerodynamic conversion process represents extraction of the kinetic energy contained in the moving air masses that interact with WT blades. The study uses simplified aerodynamic model in which the air mass interacts with every blade surface equally, and therefore extracted power depends only on flow rate of whole air mass, i.e. wind speed.

Kinetic energy exists only in the moving air and can be determined according equation:

$$E_k = \frac{1}{2} m v_w^2 \tag{2.1}$$

where m – is the air mass and v_w – is the wind speed. The full power consisting in wind is calculated by derivation of the wind kinetic energy with respect to time:

$$P_w = \frac{dE_k}{dt} = \frac{1}{2} \dot{m} v_w^2. \tag{2.2}$$

However, only a part of wind power is applied to wind turbine blades and then transferred into the rotational motion of wind turbine rotor. Therefore, useful wind mass flow rate can be represented as:

$$\dot{m} = \rho A_r v, \tag{2.3}$$

where ρ – is the air density, A_r – is the area, swept by the rotor. Wind power available for capturing by WT can be estimated as follows:

$$P_w = \frac{1}{2} \rho A_r v^3. \tag{2.4}$$

The key characteristic of wind power generation is the power coefficient C_p, which means the relation between actually captured mechanical power P_{mec} and the maximum available power of the wind P_w. Power coefficient is expressed as:

$$C_p = \frac{P_{mec}}{P_w}. \tag{2.5}$$

According to Betz's law, power coefficient for horizontal-axis WTs cannot exceed the value of 16/27 (59.3%). (Burton, Jenkins, Sharpe, & Bossanyi, 2011). Actual mechanical power captured by WT blades is:

$$P_{mec} = C_p P_w = \frac{1}{2} C_p \rho A_r v^3. \tag{2.6}$$

Power coefficient depends on two factors – wind turbine tip speed ratio λ and blades pitch angle β. WT tip speed ratio is a relation between tangential speed of the blade tip v_t and the wind speed:

$$\lambda = \frac{v_t}{v_w}. \tag{2.7}$$

Tangential speed of the blade tip is a product of the rotor radius r_r and its rotational speed Ω_r. Therefore, tip speed ratio may be rewritten as follows:

$$\lambda = \frac{\Omega_r r_r}{v_w}. \tag{2.8}$$

It is necessary to protect wind turbine from exceeding stresses on high wind speeds. It is achieved by limiting the power caught by blades via regulation of the blades pitch angle β.

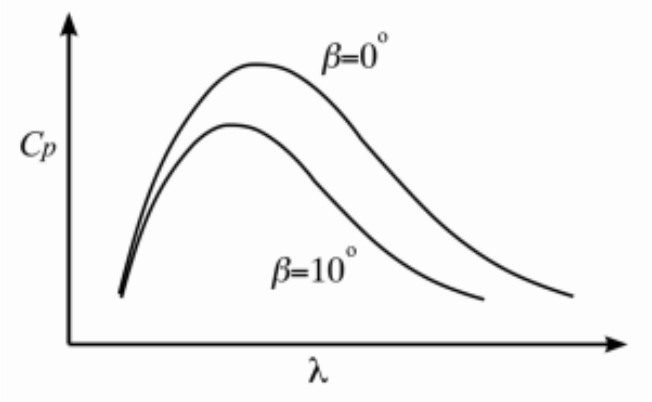

Figure 2.3. Typical Cp curve.

Typical C_p curve is illustrated in Figure 2.3. It can be observed from the figure that the maximum power coefficient and therefore the maximum power, generated by wind turbine, is obtained with some special value of tip speed ratio, which is called optimal tip speed ratio. The first principle of DFIG control can be derived from here: control system should maintain rotor speed in such way to keep the tip speed ratio equal to its optimal value. The optimal tip speed ratio is a key characteristic of the WT design.

PLECS DFIG model contains an aerodynamic model, which is represented as look-up table. The look-up table takes wind speed and rotor rotational speed as input data and produces wind torque that is applied to blades as output. The look-up table data is obtained on the basis of typical $C_p(\lambda)$ curve and is shown in Figure 2.4.

However, the data is only provided for speeds below 12 m/s and torque obtained on higher speeds increases linearly, which makes it impossible to investigate wind turbine behavior on higher wind speeds. Application of the look-up table for wind speeds up to 30 m/s and different rotor speeds range is presented in Figure 2.5a. It can be seen from the figure that linear gain on wind speeds higher than 12 m/s on high rotor speed leads output torque to achieve enormous values, while on lower rotor speeds the torque becomes negative, which is untrue in practice. For wind speeds higher than 12m/s the data was extrapolated and exponentially corrected. Output torque of the corrected aerodynamic model is illustrated in Figure 2.5b.

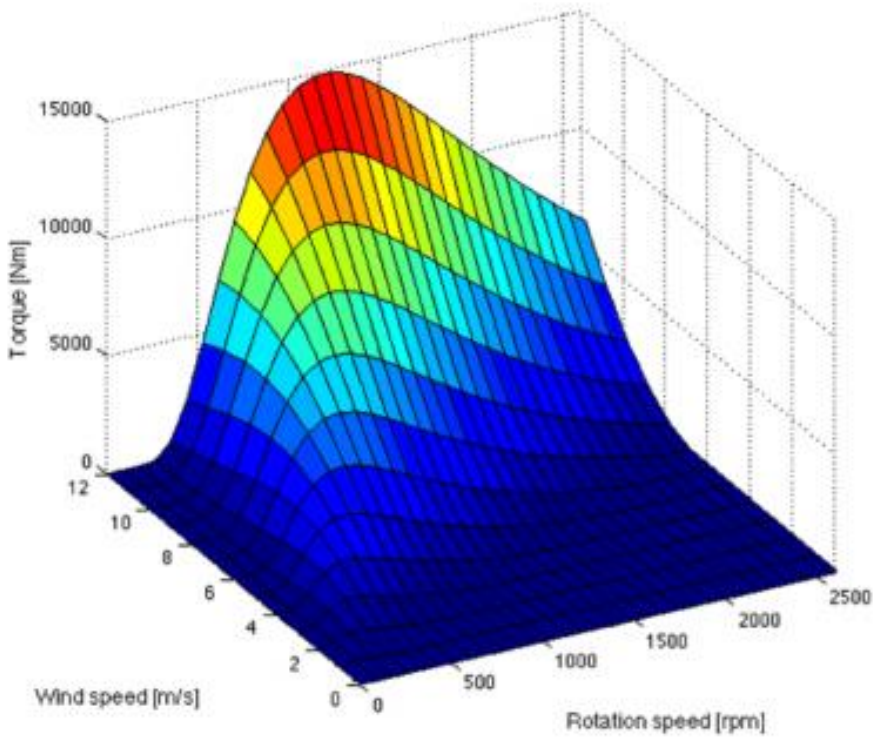

Figure 2.4. PLECS built-in aerodynamic look-up table data (Luo, 2013)

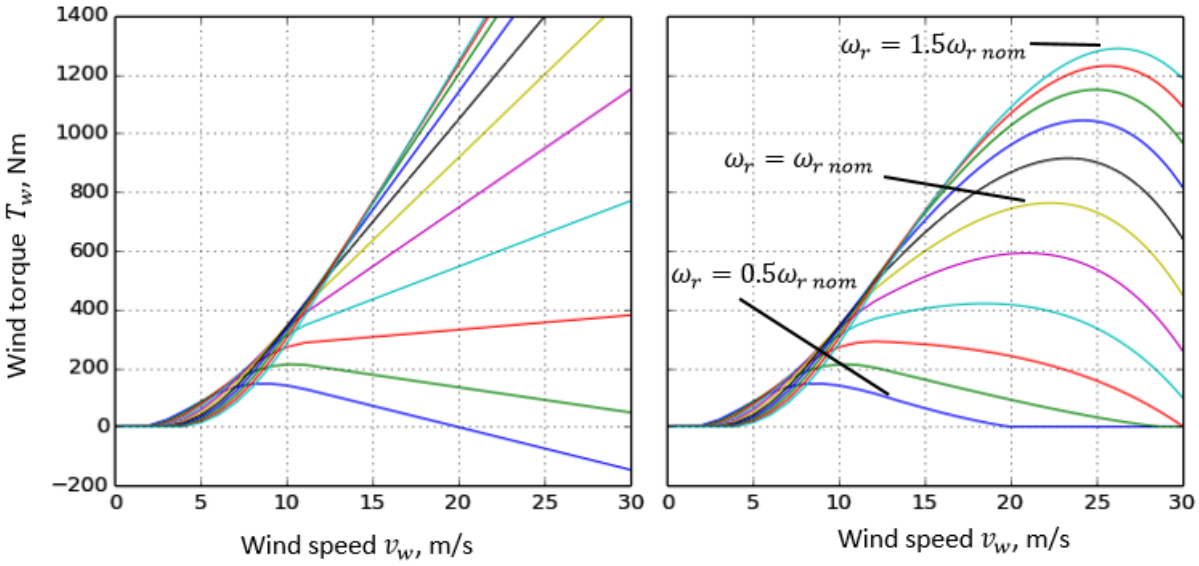

Figure 2.5. Original (a) and corrected (b) aerodynamic model output

2.3 Mechanical system

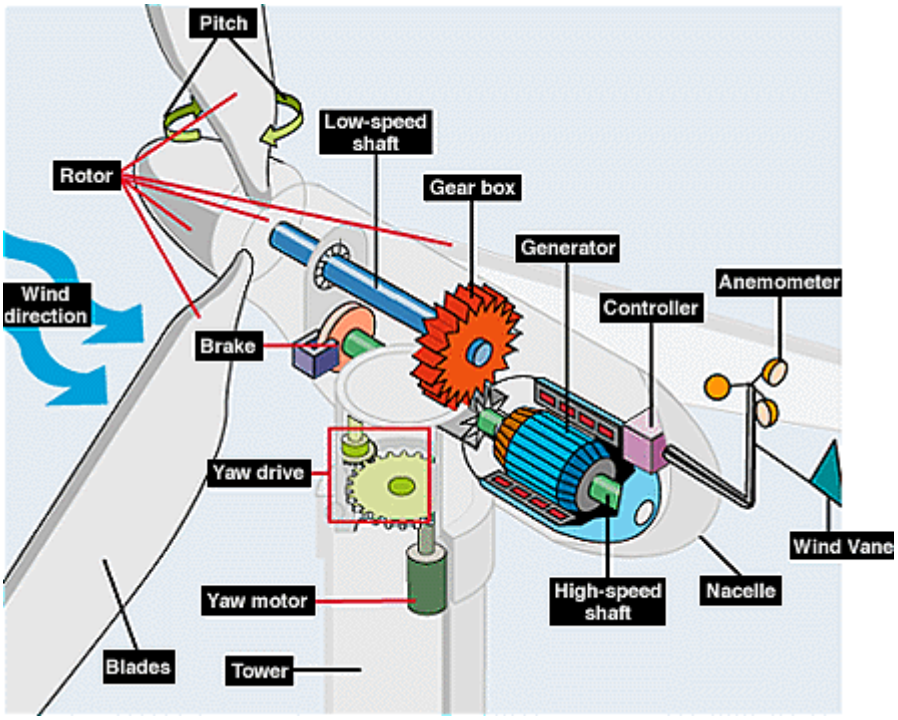

Figure 2.6. WT mechanical system.

The mechanical system of the real WT is represented in Figure 2.6. Mechanical links that mostly define WT dynamics and therefore necessary to be considered in the model are the WT low-speed shaft with blades and rotor placed on it, the gearbox that transfers rotational movement of low-speed shaft into rotational movement of the generator high-speed shaft, and the high-speed shaft with generator. Blades pitch angle is also a necessary thing to be considered as it directly determines amount of power caught from the wind. Therefore, the most important aspect of mechanical system, which has to be simulated, is the transformation of torque applied to blades on the low-speed shaft to torque applied on the high-speed shaft with generator.

There are several approaches to model the mechanical part of WT divided according to their complexity. WT mechanical system can be modelled as two-mass, three-mass or six-mass systems (Muyeen, Tamura, & Murata, 2009). In the PLECS DFIG WT model the six-mass mechanical system is used and therefore utilized for study purposes

In the six-mass mechanical model there are six inertias considered: each blades inertia, which are assumed to be equal – J_b, hub inertia – J_h, gearbox inertia – J_{GB} and generator's rotor inertia – J_R. ω_{b1}, ω_{b2}, ω_{b3}, ω_h, ω_{GB}, ω_R represent corresponding each blade, hub, gearbox and generator's rotor angular velocities. Each mass unit position is represented by its angular displacement (indexes further are similar to above) – θ_{b1}, θ_{b2}, θ_{b3}, θ_h, θ_{GB}, θ_R. Spring constants k_{gbg}, k_{hgb}, k_{bh} represent stiffness between adjacent masses. Mutual damping between adjacent masses is expressed by damping coefficients: B_{gbg}, B_{hgb}, B_{bh}. Losses of mechanical interaction are expressed by friction coefficients: D_b, D_h, D_{GB}, D_R.

The model takes torque generated by aerodynamic model as input for each blade and produces torque and angular speed for generator as output. It is assumed that the aerodynamic torques acting on the hub and gearbox are zero. The differential equations representing six-mass mechanical model dynamics can be achieved according to the Newton's second law for rotational system.

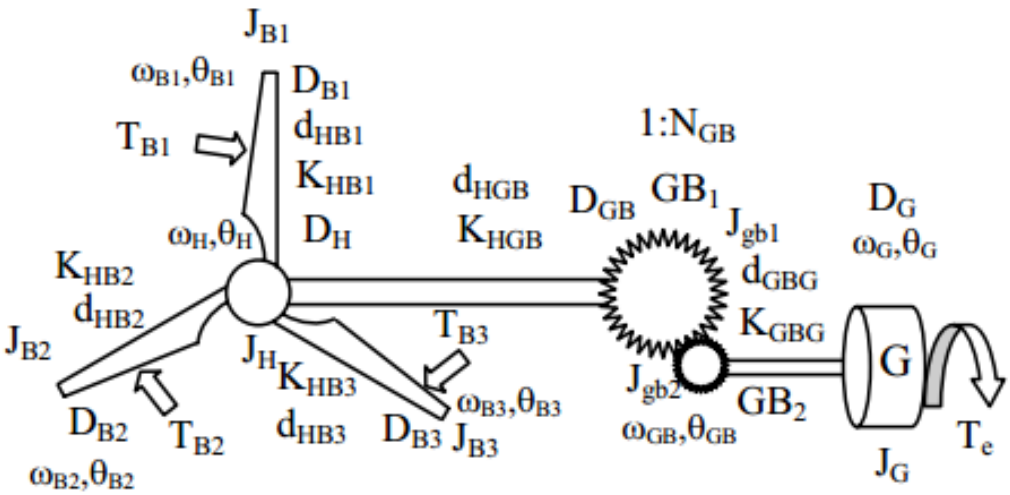

Figure 2.7. Drivetrain six-mass system representation. (Muyeen, Tamura, & Murata, 2009)

PLECS library contains main mechanical elements, such as inertial elements, torsion springs, rotational dampers and so forth, which allows to simulate mechanical interactions in the WT system. The connection of mechanical elements in the PLECS model is shown in Appendix 1.

The DFIG WT is simulated in PLECS with parameters given in Table 2.1. Their estimation is given in (Luo, 2013).

Table 2.1. Mechanical parameters for PLECS simulation of WT. (Luo, 2013)

Rotor inertia J_r	75 kgm^2
Gearbox inertia J_G	4.26×10^5 kgm^2
Hub inertia J_h	6.03×10^4 kgm^2
Blade inertia J_b	1.13×10^6 kgm^2
Rotor friction D_r	0.81 Nms/rad
Gearbox friction D_G	1.78×10^4 Nms/rad
Hub friction D_h	8.11×10^3 Nms/rad
Blade friction D_b	1.08×10^3 Nms/rad
Gearbox to rotor stiffness k_{gbg}	4.67×10^7 Nms/rad
Hub to gearbox stiffness k_{hgb}	13.9 Nms/rad
Blade to hub stiffness k_{bh}	10.7 Nms/rad
Gearbox to rotor damping B_{gbg}	810 Nms/rad
Hub to gearbox damping B_{hgb}	2.84×10^6 Nms/rad
Blade to hub damping B_{bh}	3.24×10^6 Nms/rad

2.4 Electrical circuit

The entire electrical circuit is shown in Figure 2.8. Every modelled part of it is described in the next sections.

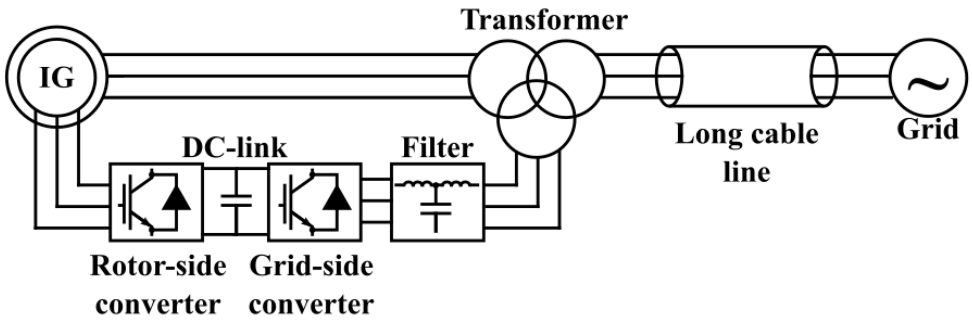

Figure 2.8. Model of the DFIG electrical circuit.

2.4.1 Generator

The generator of considered WT is a wound-rotor induction generator, which means that both stator and rotor windings are connected to the grid. Stator connects directly to the grid, while rotor connects to the grid via power converter.

The generator is modelled according to traditional fourth-order equations of the generalized induction machine in stator coordinates. Vector representation of the DFIG in stator coordinates is achieved by Clarke transformation. Clarke transformation provides representation of any three-phase system as two-phase orthogonal system according to given equations:

$$\begin{bmatrix} x_\alpha \\ x_\beta \\ x_\gamma \end{bmatrix} = \frac{2}{3} \begin{bmatrix} 1 & -\frac{1}{2} & -\frac{1}{2} \\ 0 & \frac{\sqrt{3}}{2} & -\frac{\sqrt{3}}{2} \\ \frac{1}{2} & \frac{1}{2} & \frac{1}{2} \end{bmatrix} \cdot \begin{bmatrix} x_a \\ x_b \\ x_c \end{bmatrix}, \tag{2.9}$$

Where x_a, x_b, x_c are the values given in three-phase *abc* frame; x_α, x_β are coordinates in two-phase αβ plane; x_γ is the zero-sequence component. Zero-sequence component x_γ only exists in non-symmetrical four-wire systems and is not considered further.

Then vector representation in stationary reference frame is given as follows:

$$\overline{x} = x_\alpha + j x_\beta \tag{2.10}$$

Equivalent IG circuit in stator coordinates is shown in Figure 2.9.

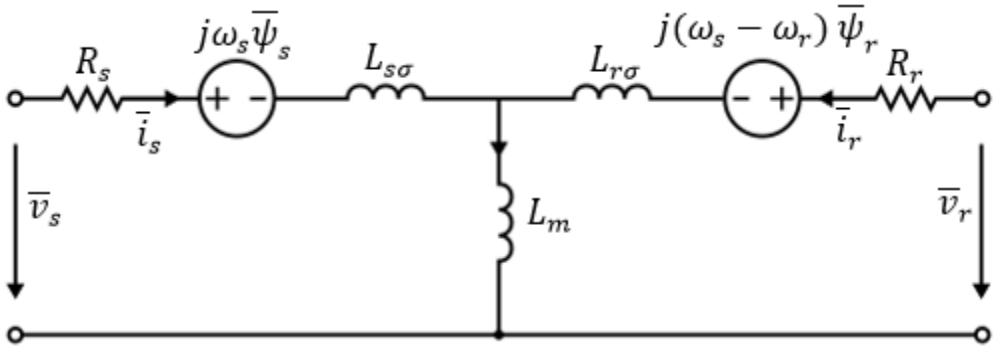

Figure 2.9. DFIG equivalent circuit in vector representation.

Voltages equations according to equivalent circuit of the DFIG are expressed as follows:

$$\begin{aligned}\overline{v}_s &= R_s\bar{i}_s + \frac{d\overline{\psi}_s}{dt} - j\omega_s\overline{\psi}_s \\ \overline{v}_r &= R_r\bar{i}_r + \frac{d\overline{\psi}_r}{dt} - j(\omega_s-\omega_r)\overline{\psi}_r\end{aligned} \tag{2.11}$$

where $\overline{v}_s$, $\overline{v}_r$ are stator and rotor voltages; $\overline{\psi}_s$, $\overline{\psi}_r$ are stator and rotor fluxes; $\bar{i}_s$, $\bar{i}_r$ are stator and rotor currents; R_s, R_s are stator and rotor resistances; ω_r is the rotor angular speed. Stator and rotor fluxes of the DFIG are given by:

$$\begin{aligned}\overline{\psi}_s &= L_{\sigma s}\bar{i}_s + L_m\bar{i}_r \\ \overline{\psi}_r &= L_{\sigma r}\bar{i}_r + L_m\bar{i}_s\end{aligned} \tag{2.12}$$

Where $L_{\sigma s}$, $L_{\sigma r}$ are stator and rotor leakage inductances; L_m is the mutual inductance.

Mechanical dynamics of the IG are given as follows:

$$\begin{aligned}\frac{d\omega_r}{dt} &= \frac{p}{2J}(T_e - F\omega_r - T_m) \\ \omega_s &= p\omega_m\end{aligned} \tag{2.13}$$

Where J is the moment of inertia of the IG rotor; T_m is the mechanical torque which is applied to the IG shaft by drivetrain; T_e is the produced electromagnetic torque; ω_r is the mechanical

rotor speed on the high-speed side of drivetrain; F is the friction coefficient; p is the number of IG poles.

Electromagnetic torque in vector representation is given as follows:

$$T_e = 3n_p \mathrm{Im}[\overline{\psi}_s \bar{\imath}_r^*] \quad (2.14)$$

PLECS contains built-in wound rotor model block: Induction Machine (Slip Ring). This block has 6 electrical inputs: 3 phases of stator and 3 phases of rotor. Rotor terminals are accessed by slip rings. The block also has an electrical torque input. Machine can work in both generator and motor modes depending on sign of torque signal (positive leads to motor mode). The magnetic saturation of both rotor and stator circuits is neglected. IG was simulated with parameters given in Table 2.2

Table 2.2. Electrical parameters for PLECS simulation of the IG. (Luo, 2013)

Pole pairs p	2
Turns ratio n_s/n_r	1/2.6
Stator leakage $L_{s\sigma}$	0.12 mH
Rotor leakage $L_{r\sigma}$	0.05 mH
Mutual inductance L_m	2.9 mH
Stator resistance R_s	0.022 Ohm
Rotor resistance R_r	0.0018 Ohm

2.4.2 Power converter

DFIG WT contains a back-to-back power converter in the rotor circuit. The power converter consists of two three-phase two-level IGBT-based inverters with connected DC-sides via DC-link capacitor. Power converter electrical circuit is shown in the Figure 2.6.

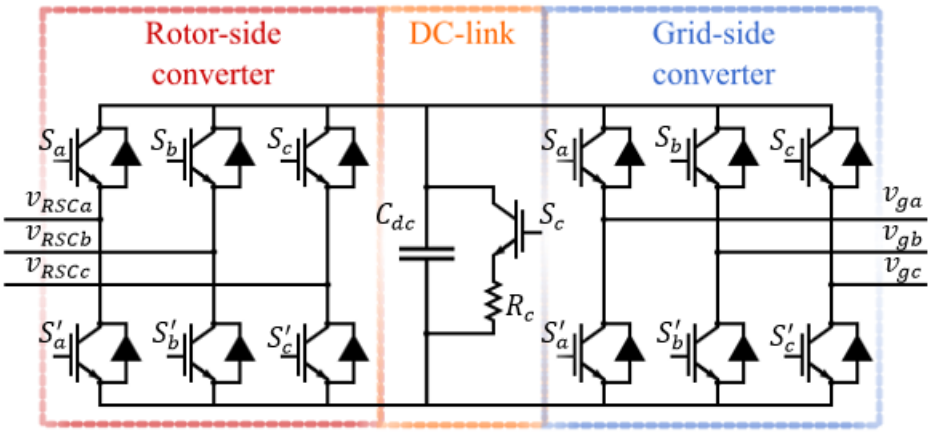

Figure 2.6. Back-to-back power converter

Two-level bridge connects every phase of its AC side with the positive or negative terminal of the DC-link capacitor, so in each phase applied voltage by the inverter can be only positive or negative value of the DC-link voltage.

Thermal and switching losses of bridges are beyond the scope of the thesis and therefore simplified model of bridges is considered. Hence, voltages v_{Sa}, v_{Sb}, v_{Sc} applied to every phase of the inverter AC side depend only on IGBT switching functions s_a, s_b, s_c and the DC-link voltage v_{dc}:

$$\begin{aligned} v_{Sa} &= s_a v_{dc} \\ v_{Sb} &= s_b v_{dc} \\ v_{Sc} &= s_c v_{dc} \end{aligned} \tag{2.15}$$

The switching function is considered for one leg of the inverter and equals to 1 if the top IGBT is on (conducts) and bottom IGBT is off, so positive DC-link voltage is applied; and switching function equals to -1 otherwise. Switches of one inverter leg therefore work as complementary pair.

Because of only two levels of voltage can be applied to each phase of the inverter, the filter should be placed on the AC side to smooth currents ripples. However, AC side of rotor side converter (RSC) – is connected to the IG rotor windings because of rotor windings inductances naturally act as a smoothing current filters.

The energy, which is stored in the capacitor is written as:

$$E_c = \int Pdt = \frac{1}{2} C V_{dc}^2 \tag{2.16}$$

DC-link also contains a chopper circuit with shunting resistor, activated by the transistor. The purpose of this circuit is to limit DC-link voltage while forcing part of the DC-link power to be dissipated as heat on the shunt resistor R_c. That prevents overvoltage of the DC-link capacitor that can be caused by emergency operation modes, such as voltages sags.

PWM-led power converter produces rapidly changing pulses of applied voltage to the grid side that will produce current ripples affecting grid power quality. Therefore, it is required to smooth current waveform on the output of converter by placing filter between grid side converter (GSC) and transformer winding. There are several alternatives of filter designs, most common examples of which is the pure inductive L-filter and the LCL-filter. The LCL filter is used in the DFIG WT Plecs model, as it is more often being used in modern applications due to lower price and weight in comparison with the pure inductive filter of similar characteristics. However, existence of both L and C elements in the circuit leads to resonance effects on some frequencies and control system should be able to eliminate these effects. Quite easy damping of the resonance currents can be implemented by measuring them from the filter and considering in the control law. The structure of the LCL filter is presented in the Figure 2.1. Sample LCL-filter design is described in (Reznik, Simoes, Al-Durra, & Muyeen, 2014).

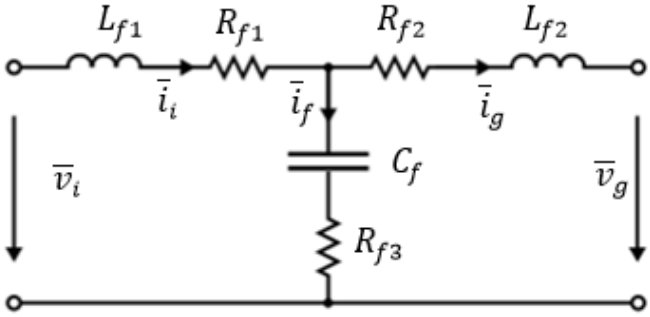

Figure 2.7. LCL filter circuit

Differential equations of the LCL filter in vector representation are given as follows:

$$\frac{d\overline{v}_f}{dt} = \frac{\overline{i}_i - \overline{i}_g}{C_f}$$

$$\frac{d\overline{i}_i}{dt} = \frac{1}{L_{f1}}\left(\overline{v}_i - \overline{v}_f - R_{f3}\left(\overline{i}_i - \overline{i}_g\right) - R_{f1}\overline{i}_i\right) \tag{2.17}$$

$$\frac{d\overline{i}_g}{dt} = \frac{1}{L_{f2}}\left(\overline{v}_f - \overline{v}_g + R_{f3}\left(\overline{i}_i - \overline{i}_g\right) - R_{f2}\overline{i}_g\right)$$

Where $\overline{i}_i$ is the current vector flowed from AC side of the inverter; $\overline{i}_g$ is the current vector flowed to the grid; $\overline{i}_f$ – current vector flowing through the capacitor C_f; $\overline{v}_i$ is the voltage vector applied on the AC side of inverter; $\overline{v}_c$ is the voltage vector across filter capacitors; $\overline{v}_g$ is the grid voltage vector; C_f is the filter capacitance; R_1, R_2 are resistances of serial resistors from the inverter and grid side; R_f is the resistance of shunt (damping) resistor; L_1, L_2 are inductances of serial windings. Vector quantities are written according to (2.10) and (2.9).

2.4.3 Connection to the grid

Both rotor circuit with power converter and stator windings are connected to the grid via three-winding transformer. Such transformer is required because it minimizes the rotor current without exceeding the maximum available rotor voltage. In our case the voltage of the rotor-side transformer winding is 400 V and stator-side is 690 V.

WT requires some special landscape to be placed for being effective in power generation. It leads to usual placing of WT on some significant distance from the transformer substation, which connects WT to the grid (in grid-oriented operation) or enterprise distribution network (in standalone operation).

Grid-side windings of the transformer are connected to a long cable line, which has length of 20 km in presented model. Voltage amplitude on the medium voltage side of transformer achieves value 10 kV. Long cable line is modelled with built-in PLECS block that models line with distributed parameters, which considers travelling wave effect and consequent power losses. The grid is modelled as ideal per-phase controlled voltage sources, which allows to

simulate every kind of grid fault necessary for the study purpose. However, it should be noted, that in PLECS line with distributed parameters forbids to simulate unbalanced conditions.

3 CONTROL OF THE DFIG WT

3.1 Control system overview

As DFIG is operated by the rotor converter, the DFIG WT control system contains outer controller, which purpose is to produce references for basic WT parameters, such as rotor speed and reactive power reference for both DFIG and GSC. DFIG control system consists of two controllers. The purpose of controllers is to operate switches of the IGBT bridges in rotor circuits in appropriate way to make possible the DFIG to follow the required reference values.

In the paragraph 2.1, it was mentioned that primary control principle of the WT is to maintain necessary rotor speed on different wind speeds. The RSC controller suits this task by applying different voltages to the IG rotor. Its operability primarily depends on the DC-link voltage stability, which is provided by the GSC controller. These principles determine the active power flow between DFIG system and the grid. However, each of the controllers also should provide reactive power control in order to both compensate the IG reactive power consumption and fulfill power quality requirements of the consumer.

Therefore, general structure of the DFIG WT control system is shown in the Figure 3.1. The overall control system contains three controllers:

- WT controller provides references for general parameters of the WT, such as rotor speed, reactive power reference and pitch angle correction.
- RSC controller operates the DFIG by controlling the RSC IGBT bridges in appropriate way to make the DFIG follow rotor speed and reactive power references.
- GSC controller operates GSC in order to maintain necessary level of the DC–link voltage as well as to follow reactive power reference.

Control structure of each power converter controller usually can be divided in two main components. First is the control strategy, which provides set of calculations to obtain reference voltages that should be produced by the power converter on the AC-side. The second is the switching algorithm that provides IGBT switches operation in order to follow reference voltage

on the AC-side of converter. There are several switching algorithms mainly used in the control systems that are described in literature: sinusoidal PWM, space vector modulation (SVM) and switching tables. This chapter is focused on the derivation of control strategy for the DFIG, so detailed description and implementation of switching algorithms is beyond the scope of thesis and may be found in literature, for example: (E. Hendawi, 2010). In our study, the SVM algorithm is used to control both RSC and GSC switches.

There are currently two well-known control strategies for the three-phase power converters – vector control and direct torque control (DTC) – for machine-side inverters, or its similar implementation – direct power control (DPC), which is suitable for both grid-side and machine-side inverters. Vector control calculations are processed in rotational reference frame, which is synchronized with some reference vector. Vector control systems usually contains current control loops with PI or PID regulators and outer control loops with P or PI regulators to provide reference value control, such as power or torque. DTC algorithm is based on direct calculations of the torque reference, while DPC calculations are made according to the instantaneous power theory. Both DTC and DPC algorithms can be implemented in both stationary and synchronous reference frames and. Vector control strategy is used in this work to operate both converters and this chapter is devoted to derivation of control laws and principles of vector control implementation. Other control systems for the DFIG WT can be found in (Cartwrigh, 2006).

DFIG WT vector control hierarchy and measurements and control signals diagram is presented in the Figure 3.1. Every inverter in rotor circuit has assigned controller – RSC and GSC controllers. Each controller has inner current loops with PI regulators and outer loops for reactive and active power control. RSC and GSC controllers obtain references from the WT controller, which depending on wind speed obtained from the anemometer produce rotor speed or torque reference for the RSC controller and depending on the external reactive power reference or grid voltage controller produces reactive power reference for both RSC and GSC. Each block of the control system will be discussed in details through this chapter except the pitch angle controller and maximum power point tracking block, which are introduced in the paragraph 4.3 and 4.4.

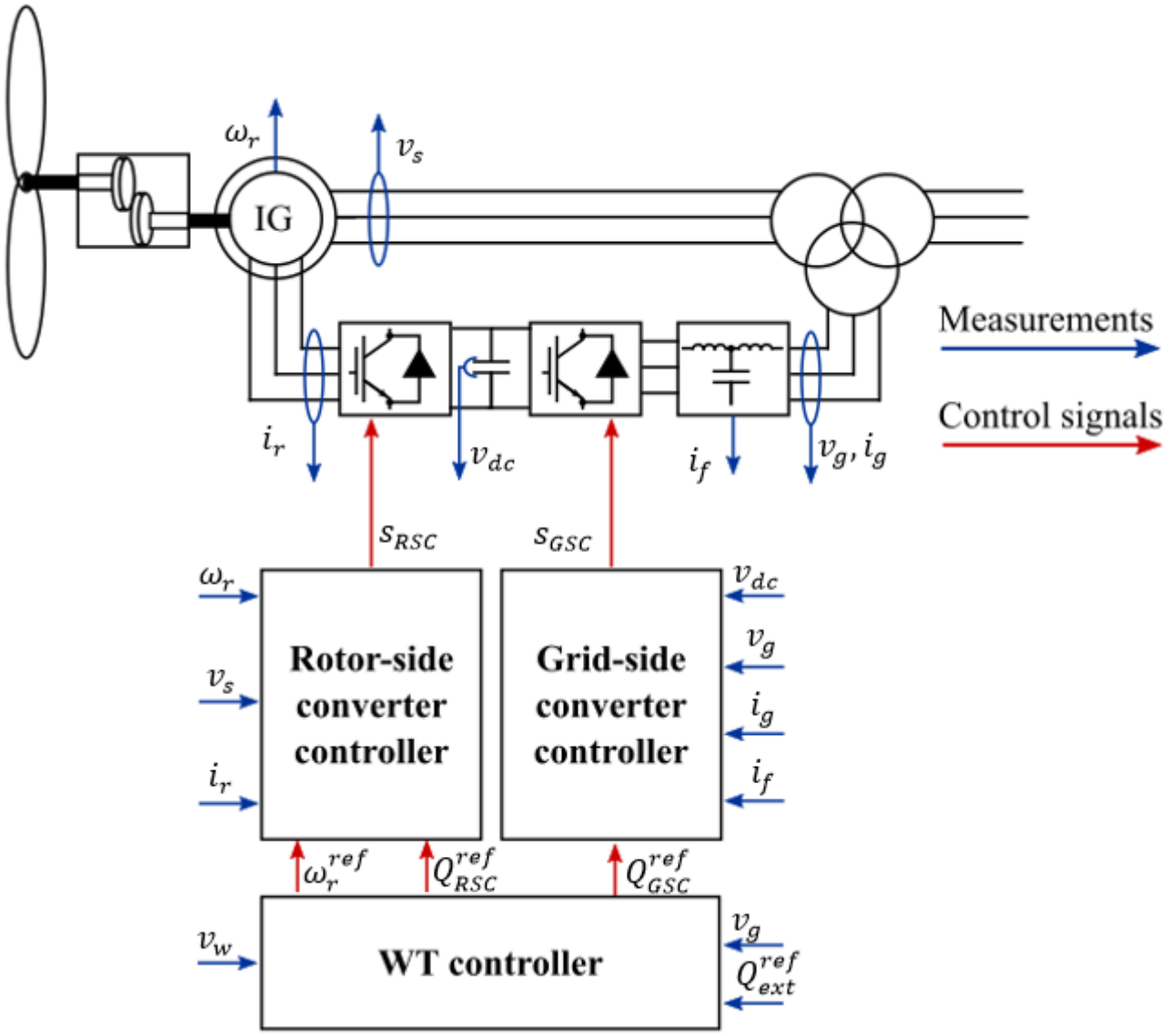

Figure 3.1. DFIG WT control hierarchy.

3.2 RSC vector control system

The main purpose of the RSC controller is to control the active and reactive power produced by the DFIG wind turbines. DFIG circuit power flows are explained in detail in chapter 4. At this moment it is essential to know that according to aerodynamic model expressed in paragraph 2.2 active power produced by the DFIG mostly relates on its rotor speed. RSC should maintain active and reactive power generation by applying voltages to the DFIG rotor, therefore, control law is expected to be expressed as stator active and reactive power in terms of voltages applied to the DFIG rotor.

Vector control system uses the IG electrical model (2.12) of the thesis. However, for control purposes instead of stationary frame, the synchronous reference frame is usually preferred. Such approach has two main advantages:

- In steady-state operations the control quantities become constant and therefore easier controlled
- Its natural decoupling of necessary control values, for example in terms of active and reactive components of voltages and currents.

Dq synchronous reference frame orientation is achieved by applying Park transform to stationary vector coordinates. For placing *d*-axis along the reference vector, the Park transformation is given as:

$$\begin{bmatrix} x_d \\ x_q \end{bmatrix} = \begin{bmatrix} \cos\theta & \sin\theta \\ -\sin\theta & \cos\theta \end{bmatrix} \cdot \begin{bmatrix} x_\alpha \\ x_\beta \end{bmatrix} \tag{3.1}$$

Where θ is the angle of the rotating reference vector; x_d, x_q are the d (direct) and the q (quadrature) coordinates in synchronous reference frame. Rotation angle can be expressed in terms of the synchronous frame angular frequency ω_{dq} and its starting displacement θ_0 as follows:

$$\theta = \omega_{dq} t + \theta_0 \tag{3.2}$$

3.2.1 Stator flux oriented reference frame

The usual approach in a control law design for IM is to simplify control algorithm by synchronization of the *dq* reference frame with one of the machine vector values: stator voltage, air gap flux or stator flux. In this work the stator flux oriented (SFO) control approach is described as the most common variant of the DFIG control. Different alignments of synchronous reference frame are described in (Petersson, Harnefors, & Thiringer, 2004).

Synchronization of *dq* reference frame with stator flux is achieved by substitution of stator flux angular speed ω_ψ and initial displacement $\theta_{0\psi}$ to the Park transform equations and DFIG vector model (2.12). Applying SFO Park transform to the DFIG electrical model in stationary coordinates (2.12) gives for voltages:

$$\begin{aligned} v_{sd} &= R_s i_{sd} + \frac{d\psi_{sd}}{dt} + \omega_\psi \psi_{sd} \\ v_{sq} &= R_s i_{sq} + \frac{d\psi_{sq}}{dt} - \omega_\psi \psi_{sq} \\ v_{rd} &= R_r i_{rd} + \frac{d\psi_{rd}}{dt} + (\omega_\psi - \omega_r)\psi_{rq} \\ v_{rq} &= R_r i_{rq} + \frac{d\psi_{rq}}{dt} + (\omega_\psi - \omega_r)\psi_{rd} \end{aligned} \tag{3.3}$$

And for flux linkages:

$$\begin{aligned} \psi_{sd} &= L_m(i_{sd} + i_{rd}) \\ \psi_{sq} &= L_m(i_{sq} + i_{rq}) \\ \psi_{rd} &= (L_m + L_\sigma)i_{rd} + L_m i_{sd} \\ \psi_{rq} &= (L_m + L_\sigma)i_{rq} + L_m i_{sq} \end{aligned} \tag{3.4}$$

Assuming ideal synchronization, the *d*-axis aligns along the stator flux vector and therefore ψ_{ds} equals to its magnitude, while stator flux *q*-axis projection ψ_{qs} will be zero. Equivalent IM circuit in SFO *dq* plane is shown in the Figure 3.2.

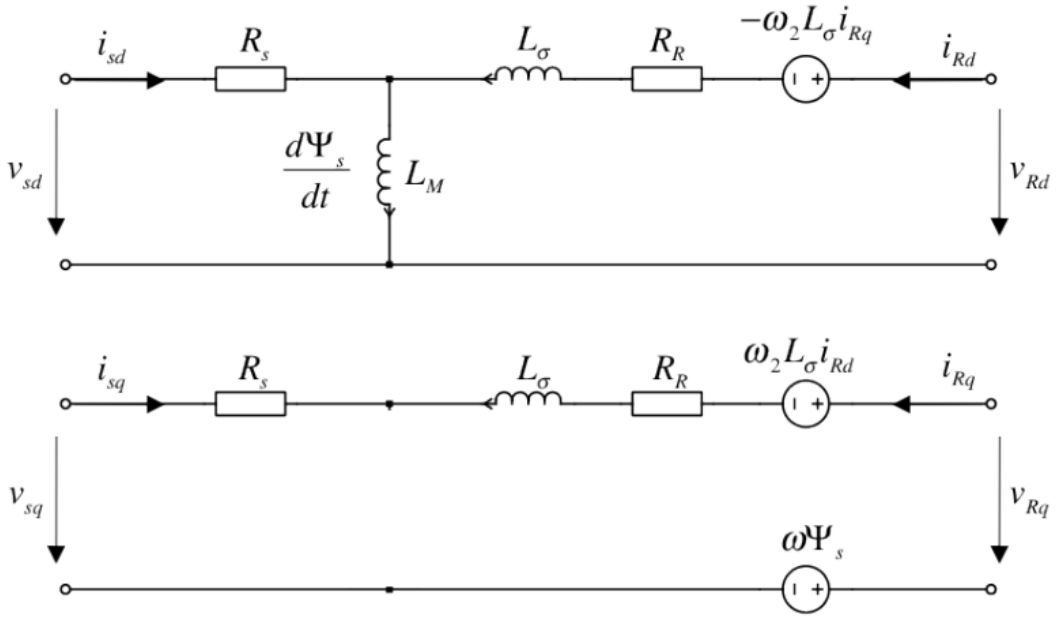

Figure 3.2. Equivalent IG circuit in SFO reference frame. (Luo, 2013)

3.2.2 Currents control loop

Currents control law expresses reference voltages in terms of reference and actual rotor currents. It is possible to obtain equations for rotor voltages by substitution of flux linkages and stator voltages equations (3.4) to the rotor voltages equations (3.3).

Solving these equations in term of rotor voltages, we can derive control law for currents control loop, which becomes:

$$\begin{aligned} v_{rd} &= (R_r + R_s)i_{rd} - \omega_r L_\sigma i_{rq} + L_\sigma \frac{di_{rd}}{dt} + v_{sd} - \frac{R_s}{L_M}\psi_{ds} \\ v_{rq} &= (R_r + R_s)i_{rq} - \omega_r L_\sigma i_{rd} + L_\sigma \frac{di_{rq}}{dt} + v_{sq} - \omega_\psi \psi_{qs} \end{aligned} \tag{3.5}$$

Where last two terms in equations describe the back EMF E, which is given as follows:

$$\begin{aligned} E_d &= v_{sd} - \frac{R_s}{L_M}\psi_{ds} = v_{sd} \\ E_q &= v_{sq} - \omega_\psi \psi_{qs} \end{aligned} \tag{3.6}$$

Inner control loops are used to maintain currents flow in DFIG rotor circuit in that way to
The key point of developing control law from new obtained model in synchronous frame is to derive currents control loops.

Hereinafter we express PI control circuits as follows:

$$k_{PI}(x^{ref} - x) = k_P(x^{ref} - x) + k_I \int (x^{ref} - x) \tag{3.7}$$

Where k_P is a proportional gain and k_I is an integral gain of PI controller, x^{ref} – reference control value, x – actual value. Control law becomes then:

$$\begin{aligned} v_{rd}^{ref} &= (R_r + R_s)i_{rd} - \omega_r L_\sigma i_{rq} + k_{PI}\left(i_{rd}^{ref} - i_{rd}\right) + v_{sd} - \frac{R_s}{L_M}\psi_{ds} \\ v_{rq}^{ref} &= (R_r + R_s)i_{rq} - \omega_r L_\sigma i_{rd} + k_{PI}\left(i_{rq}^{ref} - i_{rq}\right) + v_{sq} - \omega_\psi \psi_{qs} \end{aligned} \tag{3.8}$$

Reference voltages signals are fed to the inputs of SVM block, which controls switches states of the RSC.

3.2.1 Stator flux estimation

It can be seen from previous sections that it is necessary to know flux linkage vector for both dq-reference frame synchronization and estimation of back EMF in the currents control law. However, stator flux cannot be easily measured and should be estimated instead. There are different techniques for stator flux estimation that are described in literature, for example (Xu, De Doncker, & Novotny, 1988).

3.2.3 Speed controller

Speed controller is an external control loop of the RSC control system. Speed controller takes speed as reference signal and produces reference for active current controller as output based on simplified rotor speed dynamics expressed as follows:

$$\frac{J}{n_p}\frac{d\omega}{dt} = T_e - T_w \tag{3.9}$$

Where T_w is the torque applied to the low-speed shaft blades; T_e is the electromagnetic torque produced by the IG. Caught wind torque is obviously a non-controllable value here. Therefore, rotor speed dynamics are driven by control of electromagnetic torque T_e. Reference torque value can be obtained by rotor speed PI regulation:

$$T_e^* = k_{PI}(\omega_r^* - \omega_r) \tag{3.10}$$

The actual torque usually cannot be measured as such measurements require sophisticated and expensive sensors. Hence, reference current is calculated in open-loop manner according to:

$$i_{rq}^{ref} = -\frac{2T_e^*}{3p\psi_s} \tag{3.11}$$

3.2.4 Reactive power controller

Reactive power controller produces reference for current controller in order to achieve required reactive power reference.

Considering instantaneous power in vector notation:

$$S = 3v_s i_s^* = 3\left(R_s i_s + \frac{d\psi_s}{dt} + j\omega_s\right) i_s^* \tag{3.12}$$

Reactive power in the synchronous reference frame can be estimated as follows:

$$Q_s = 3\omega_s\left(\psi_{sd} i_{sd} + \psi_{sq} i_{sq}\right) \tag{3.13}$$

In SFO reference frame q component of flux becomes zero. Rewriting (3.13):

$$Q_s = 3\omega_s \psi_{sd} i_{sd} = 3\omega_s \left(\frac{\psi_{sd}}{L_M} - i_{rd} \right) \tag{3.14}$$

Then reference direct current component can be achieved by use of PI regulator as:

$$i_{rd}^* = \frac{\psi_{sd}}{L_M} - \frac{k_{PI}\left(Q_s^{ref} - Q_s\right)}{3\omega_s} \tag{3.15}$$

3.3 GSC vector control system

The main purpose of the GSC control system is to maintain constant DC-link voltage, which is necessary for proper operation of the RSC and overall wind turbine. It is also possible to provide reactive power to the grid from converter if it is not heavy-loaded.

GSC control system has similar vector control structure to RSC controller – so called voltage-oriented control (VOC). VOC is based on transformation of grid voltages in the point of common coupling (PCC) and currents measured at the grid-side filter from stationary ABC coordinates to *dq* reference frame, which is synchronized with PCC voltages vector.

3.3.1 Principle of GSC operation

GSC applies variable voltages to the grid and in that way it maintains the currents flow (and therefore power) between the grid and DC-link. Both GSC and the grid may be represented as controlled voltage sources, which are connected via the filter. Considering LCL-filter having no resonance currents (i.e. they are compensated be the GSC control system without ability to achieve considerable values), it can be replaced with equivalent impedance:

$$Z_f = R_f + X_f \tag{3.16}$$

Where according to circuit shown in the Figure 2.7, the LCL filter resistance is:

$$R_f = R_{f1} + R_{f2} \tag{3.17}$$

And reactance:

$$X_f = j\omega_g\left(L_{f1} + L_{f2}\right) \tag{3.18}$$

Equivalent power circuit in vector notation is represented in the Figure 3.3.

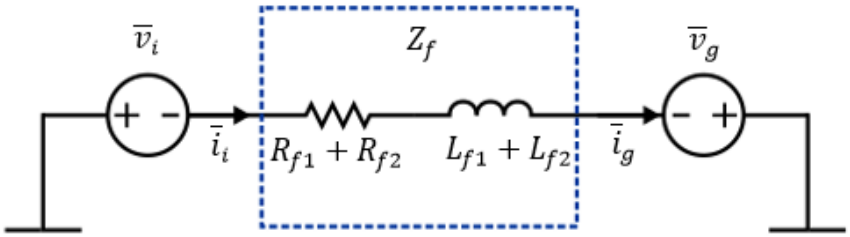

Figure 3.3. Equivalent circuit of the GSC connected to the grid.

Power balance equations applied to the circuit shown in Figure 3.1 may be written in the next form. Active current at the GSC side:

$$\overline{i}_{id} = \frac{\left|\overline{v}_g\right| sin\phi}{Z_f} \tag{3.19}$$

Reactive current at the GSC side:

$$\overline{i}_{iq} = \frac{\left(|\overline{v}_i| - \left|\overline{v}_g\right|\right) cos\phi}{Z_f} \tag{3.20}$$

Therefore, active power at the GSC side:

$$P_{GSC} = |v_i| i_{id} = \frac{|\overline{v}_i| \cdot \left|\overline{v}_g\right| \cdot sin\phi}{Z_f} \tag{3.21}$$

And reactive power at the GSC side:

$$Q_i = |v_i| i_{iq} = \frac{|\overline{v}_i|\left(|\overline{v}_i| - |\overline{v}_g| cos\phi\right)}{Z_f} \tag{3.22}$$

Presented set of equations shows that injected or absorbed from the grid active power depends on the phase angle ϕ between grid voltage $\overline{v}_g$ and GSC-produced voltage $\overline{v}_{GSC}$, while reactive power depends on the difference of in-phase voltage magnitudes $|v_{GSC}|$ and $|v_g|$ as product of $|v_g| cos\phi$ will give projection of $\overline{v}_g$ on $\overline{v}_{GSC}$. If we choose positive current direction as going from the DFIG rotor side to the grid, then positive active power will discharge DC-link capacitor, while negative active power will charge it. In that case positive reactive power will be supplied to the grid – capacitive operation, while negative reactive power will be absorbed from the grid – inductive operation.

It should be noted that in VOC reference frame subscript *d* represents active current and voltage components while subscript *q* represents reactive current and voltage components. In the RSC control system reference frame was oriented across machine flux instead, which turns direct components *d* into reactive current and voltage and quadrature components *q* into active current and voltage.

The purpose of GSC control system is to apply voltages at the grid side in a special way:

- to maintain reactive power flow by control of the GSC voltage vector in-phase magnitude;
- to maintain active power flow by control of the phase angle between GSC and grid voltage vectors.

For that purpose VOC system utilizes reference frame synchronized with the grid voltage vector. In that case, both phase and magnitude difference between voltages vectors can be controlled with DC-quantities in steady-state operation. Applying a Park transformation (3.1) to the equivalent circuit (Figure 3.3) the overall model in the dq reference frame used by GSC controller can be obtained:

$$\begin{aligned} v_{id} &= v_{gd} + \left(R_{f1} + R_{f2}\right) i_{id} - \omega_g (L_{f1} + L_{f2}) i_{iq} \\ v_{iq} &= v_{gq} - \left(R_{f1} + R_{f2}\right) i_{iq} - \omega_g (L_{f1} + L_{f2}) i_{id} \end{aligned} \tag{3.23}$$

Where q component is aligned across the voltage vector and (if the ideal synchronization considered) v_{qg} equals to voltage vector magnitude.

3.3.2 Phase-locked loop

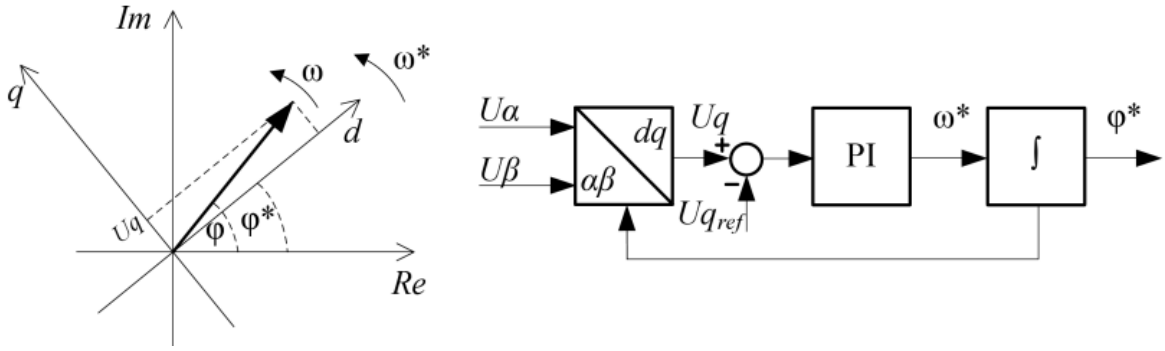

Figure 3.4. SRF-PLL algorithm.

Proper GSC operation is achieved by accurate calculation of the grid voltage phase angle that is made by phase-locked loop (PLL) circuit. There are different types of PLL algorithms described in literature. In this work the so-called SRF-PLL (synchronous reference frame PLL) technique is used, which is fast, simple and naturally produces *dq*-reference frame voltages (no need in additional transformation) so it is perfectly suited for VOC systems.

SRF PLL algorithm is based on the Park transformation of grid voltages measured in the point of common coupling (PCC) made according to (3.2.2). PLL estimates grid phase angle by forcing one of the axis components (in our case q) to follow reference value (usually zero, so another axis component will represent the vector magnitude). Error between reference and actual quantity is then controlled by PI regulator, which produces reference angular velocity as output signal. Integration of angular velocity gives a reference phase displacement that is fed to the Park transformation block. If the q-component becomes zero, the estimated angle means real grid voltage angle.

Principle of SRF-PLL operation is illustrated in Figure 3.1. SRF PLL algorithm can be written as follows:

$$\begin{aligned} \theta &= \int k_{PI}\left(v_{gq}^{ref} - v_q\right) \\ v_{gd} &= \cos\theta \cdot v_{g\alpha} + sin\theta \cdot v_{g\beta} \\ v_{gq} &= -\sin\theta \cdot v_{g\alpha} + cos\theta \cdot u_{g\beta} \end{aligned} \tag{3.24}$$

It is important to notice that such algorithm tracks angle very fast, but the accuracy of grid phase angle estimation can drastically decrease if affected by grid voltage disturbances such as unbalanced voltages or voltage waveform disturbances. To operate in such grid conditions algorithms that are more complex should be used. Examples of such algorithms are described in (Golestan S & M).

3.3.2 Currents control loop

Currents control loop equations are achieved by use of GSC-grid equivalent circuit model in the *dq* reference frame and also considering the resonance currents of the LCL filter capacitor circuit to be compensated:

$$\begin{aligned} v_{id}^{ref} &= v_{gd} + k_{PI}\left(i_{id}^{ref} - i_{GSCd}\right) - \left(R_{f1} + R_{f2}\right)i_{id} - \omega_g(L_{f1} + L_{f2})i_{iq} \\ &\quad - R_{f3}i_{fq} \\ v_{iq}^{ref} &= v_{gq} + k_{PI}\left(i_{iq}^{ref} - i_{iq}\right) - \left(R_{f1} + R_{f2}\right)i_{iq} - \omega_g(L_{f1} + L_{f2})i_{id} \\ &\quad + R_{f3}i_{fd} \end{aligned} \tag{3.25}$$

For GSC control system operation i_{id}^{ref} and i_{iq}^{ref} should be calculated by outer control loops. Produced v_{id}^{ref} and v_{iq}^{ref} values are fed to the SVM control block, which operates GSC switches in order to apply necessary voltages to the grid.

3.3.3 DC-link voltage controller

If synchronous reference frame is aligned along the grid voltage vector, the d-axis current maintains active power flow between the DC-link and grid. If we consider positive currents flow direction as flowed to the DC-link from grid, then positive values of active power will charge the DC-link, while negative currents flow will discharge it.

In order to derive DC-link voltage control law, the integral form of the capacitor voltage equation can be used:

$$v_{dc} = \frac{q_{dc}}{C} = \frac{1}{C}\int_{t_0}^{t} i_{dc}dt + V_{dc}(t_0) \tag{3.26}$$

Solving this equation for i_{dc} gives:

$$i_{dc} = \frac{dq}{dt} = C\frac{dv_{dc}}{dt} \tag{3.27}$$

Then in order to control DC-link voltage, PI regulator produces the direct axis current reference as follows:

$$i_{id}^{ref} = K_{PI}(v_{dc}^{ref} - v_{dc}) \tag{3.28}$$

3.3.4 Reactive power controller

When rotor circuit is not heavy loaded by active current, the GSC can be utilized as reactive power compensator. However, because of fact that DFIG system has a power converter rated as one third of the full WT rating, reactive power capabilities of the GSC are often used only for maintaining zero reactive power flow between the DC-link and the grid. In that case, quadrature axis current reference equates to zero:

$$i_{iq}^{ref} = 0 \tag{3.29}$$

However, in order to control reactive power, equation (3.22) can be rewritten as follows:

$$Q_i = \frac{3}{2} v_{id} i_{iq} \tag{3.30}$$

Then control law for the reactive power can be produced as follows:

$$i_{iq}^{ref} = K_{PI}(Q_i^{ref} - Q_i) \tag{3.31}$$

4 Operation of the DFIG WT

4.1 Steady-state power flows

DFIG WT electrical circuit differs from WT with full rated converters, because the power flows not only directly from generator stator to the grid but also circulates in the rotor circuit. Hence, to understand DFIG WT behavior it is useful first to investigate power flows across the DFIG WT circuits in different cases.

4.1.1 Power distribution across the circuit

Assuming lossless DFIG and power converter operation, power delivered to the grid equals to:

$$P_{out} = P_s + P_r = P_s + P_f \tag{4.1}$$

Where P_f – active power on LCL-filter.
It is also known that power in rotor circuit mainly depends on the slip:

$$P_r \approx sP_s \tag{4.2}$$

Where slip is the difference between the angular velocity of stator field rotational speed ω_s and rotor rotational speed ω_r:

$$s = \frac{\omega_s - \omega_r}{\omega_s} \tag{4.3}$$

Synchronous stator magnetic field angular frequency depends on the grid voltage frequency f_g and the number of IG poles p:

$$\omega_s = \frac{2\pi f_g}{p} \tag{4.4}$$

Synchronous speed of the DFIG according to (4.4) therefore becomes 157 rad/s. Equation (4.1) claims that slip defines possible rotor speed variations and therefore variable-speed operating range of the DFIG WT. Usually slip is supposed to be about ±30%, which provides relatively long range of operating wind speeds while power converter handles only 20-30% of rated power. Slip range ±30% determines provided rotor speeds range of the DFIG and on the high-speed shaft lies between 110 and 204 rad/s.

4.1.2 Constant wind torque

To investigate how the power is distributed across the DFIG WT circuits in steady-state operation, the simulation was made with constant wind torque applied to blades and variation of the rotor speed inside possible slip range. Wind torque value was chosen in order to produce rated WT power output at –0.3 slip value.

$$P_{m\_rated} = T_{w\_rated}\omega_{r\_max} \tag{4.5}$$

Results of the simulation are shown in Figure 4.1. The simulation of steady-state operation was made by applying the reference rotor speed ramp from 110 to 204 rad/s. The ramp slope is 0.5 rad/s, which is low enough to assume absence of transients. The figure shows that stator power remains nearly constant as well as rotor active current. The rotor power changes from –500 kW to 500 kW during the going of DFIG from sub-synchronous to super-synchronous operation. It means that ±30% slip range is provided by power converter rated 25% of the entire WT rating or 30% of the IG power rating.

Figures 4.1 also shows active voltages and currents applied to the DFIG rotor by RSC in the *dq* reference frame. It can be concluded that rotor power follows active component of voltage applied to the rotor, and stator power follows the active component of rotor current.

Calculations of slip are also presented in the Figures 4.1 based on difference of rotor speed and stator produced magnetic field frequency (4.1) and power distribution between rotor and stator

circuits (4.2). Little difference between provided slip calculations can be explained by inertial links in mechanical model that lead to rotor speed lag. The simulation confirms equation (4.1).

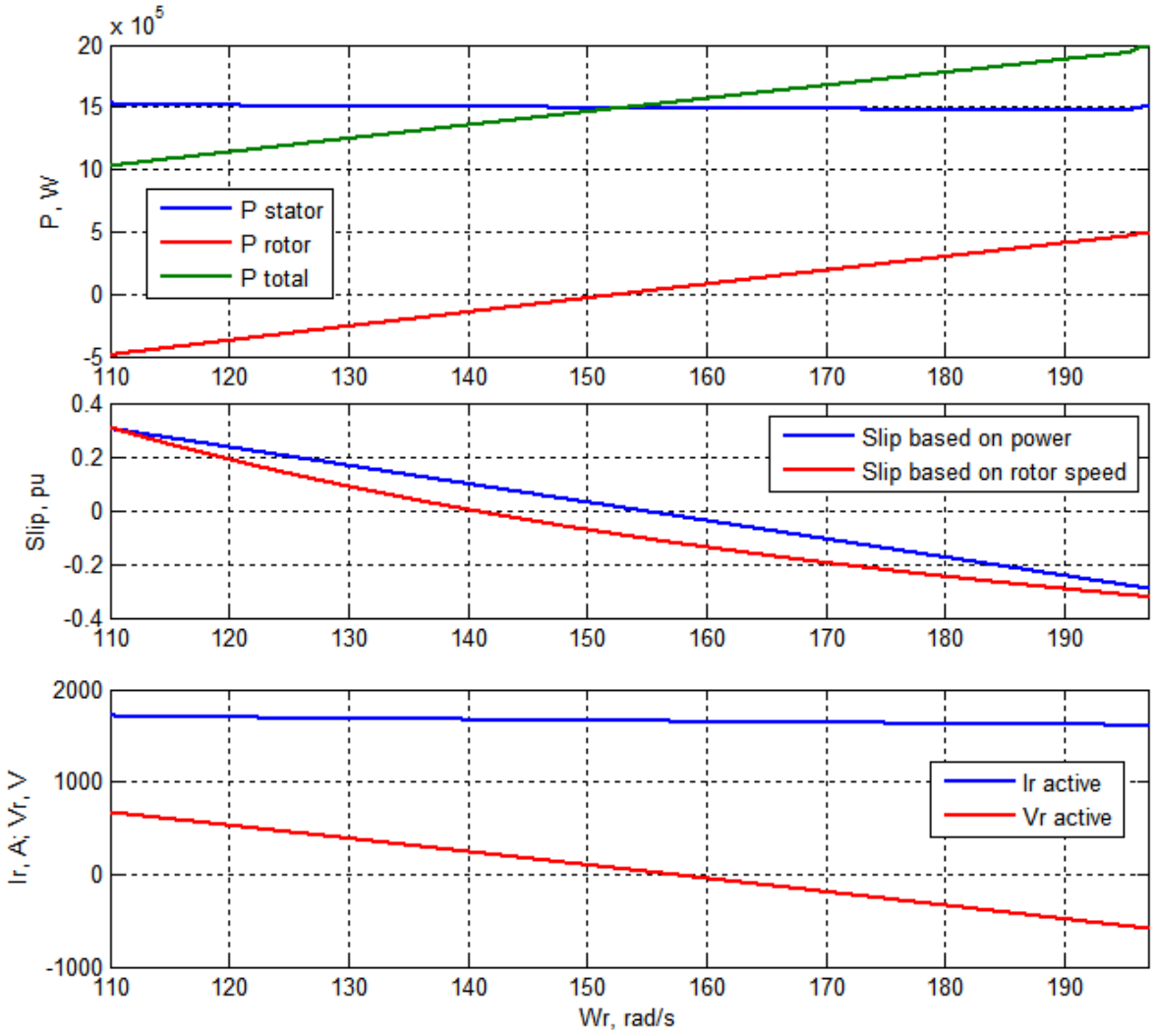

Figure 4.1. Simulation of steady-state operation with constant wind torque

4.1.3 Constant rated wind speed

Rated wind speed is usually chosen to be the most common wind speed according to statistical weather data for the region of the WT placing. Such a choice provides the best profitability of the WT. In our case rated wind speed considered to be 12 m/s. At that speed, the DFIG WT will produce rated power output equals to 2 MW.

Results of simulation are shown in Figure 4.2. In comparison with simulation results of the constant torque case, it can be observed that stator power increases with increase of the rotor speed because of increased wind torque applied to blades. It is also can be seen that to maintain 0.3 slip on the rated wind speed converter need only half of power required to maintain –0.3 slip range. We can conclude that maintaining –0.3 slip is the most intense operation for the DFIG WT.

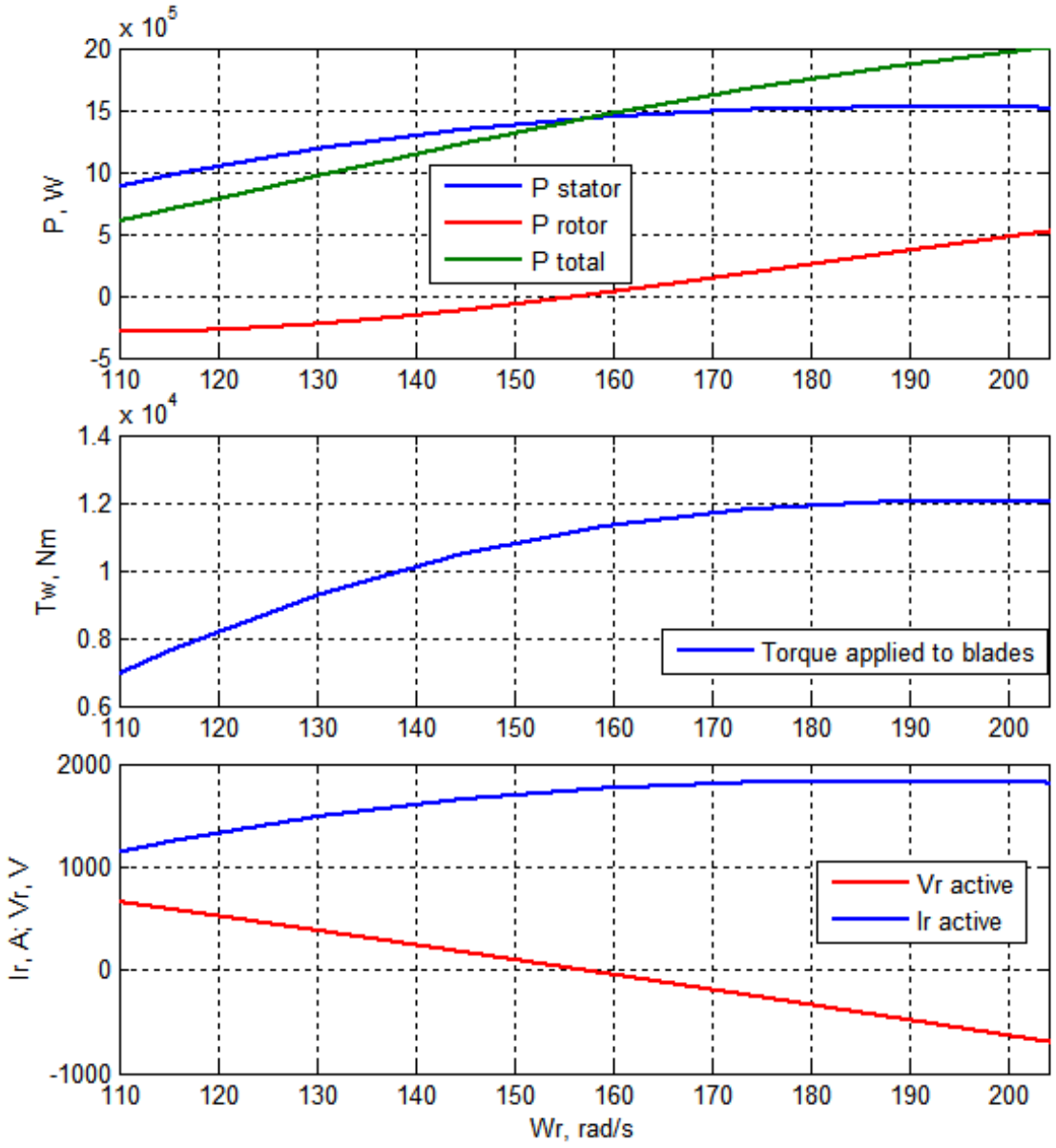

Figure 4.2. Simulation of steady-state operation with rated wind speed.

4.1.4 Constant minimal wind speed

This simulation case considers behavior of the DFIG WT on low speeds. There is a lowest wind speed below that WT cannot produce enough power and should be disconnected from the grid. Typically, value of the lowest speed is about 3–4 m/s.

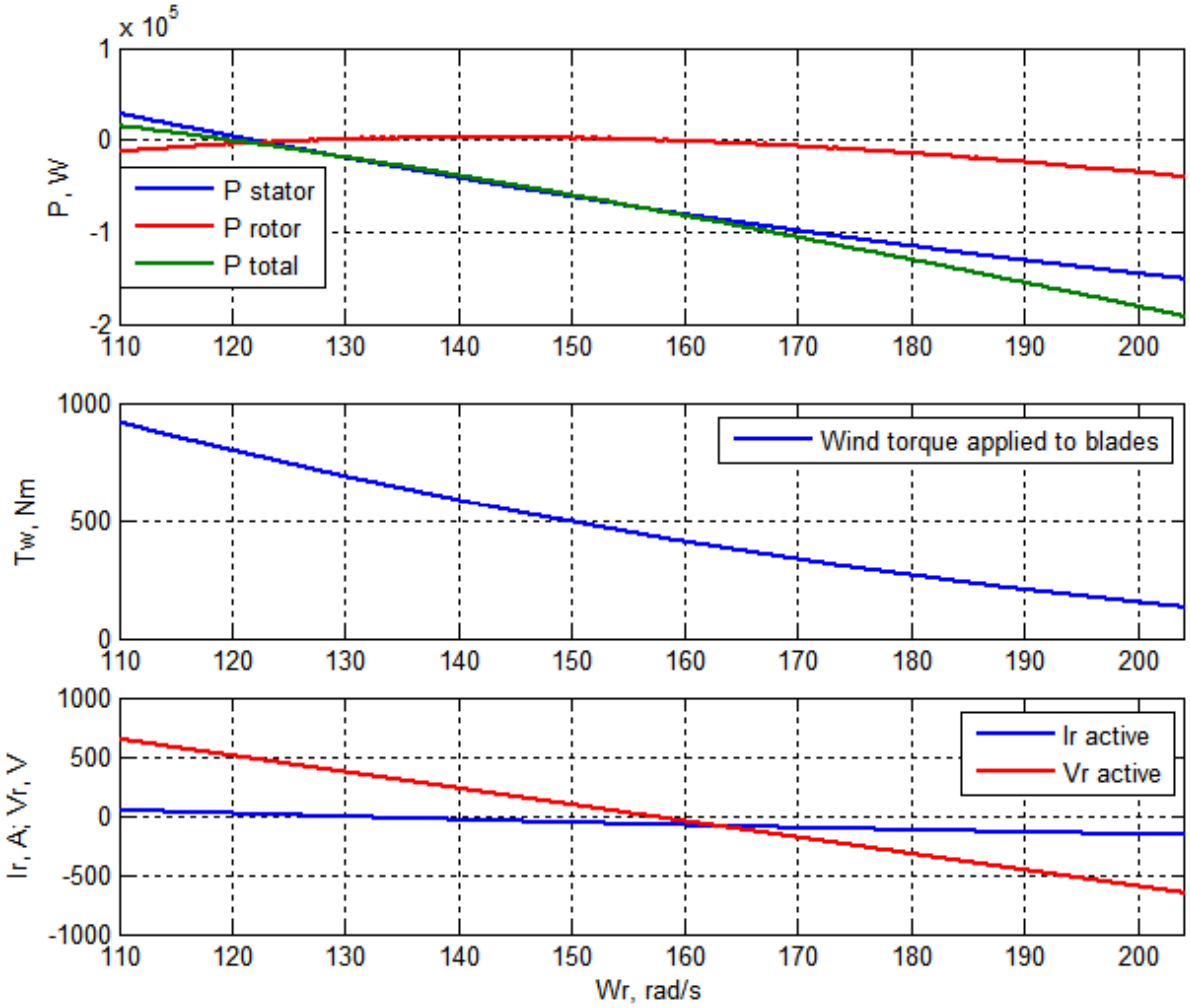

Figure 4.3. Simulation of steady-state operation with minimal wind speed.

Simulation case, considering operation on that wind speed is presented in the Figure 4.3. While on the very low speeds with slip equals to 0.3, DFIG WT still produces a little amount of power to the grid, it can be seen, that with increase of rotor speed, DFIG even goes to the motoring mode because of decrease of wind torque. During the slip range, wind torque has a positive value, however the part of generated energy is circulating in rotor circuit to maintain necessary slip, and the other part covers losses in mechanical and electrical circuits. That leads to zero

power output at low rotor speeds and further consumption of power from the grid to support rotor speed.

While on the wind speed equals to 4 m/s it is still possible to produce some useful power output at maximum negative slip value, on lower wind speeds the DFIG WT will always work in motoring mode. That describes necessity to disconnect WT from the grid at low wind speeds. One important detail can be observed from this simulation. The active component of voltage curve is the same as in rated wind speed curve, while rotor active current is close to zero.

That makes a conclusion that voltage rating of power converter determines the maximum operational slip values. On the low wind speed it also determines overall power capability of the power converter. On high wind speeds, maximum rotor speed is also limited by rotor voltage, but the maximum power handled on that slip value is determined by active current limitation of the power converter.

4.2 Optimal power point tracking

Previous set of simulation showed that on low wind speeds torque applied to blades and therefore mechanical power decreases with increase of rotor speed, while on the high wind speeds the tendency is opposite.

This is explained by the fact that different tip speed ratios lead to different wind torque. In Chapter 2 there was described aerodynamic model and introduced the optimal tip speed ratio λ_{opt} term. Maintaining this tip speed ratio across the entire variable-speed range of the DFIG WT guarantees catching maximum available power in every moment of WT variable-speed operation. In the provided diagrams optimal tip speed ratio can be seen as top of the wind torque parabolas. While on the rated wind speed optimal tip speed ratio was achieved at maximum rotor speed and therefore produced power output was increasing with increase of rotor speed, in the lowest wind speed case the top of the wind torque parabola has been left before the minimum rotor speed. Therefore, further increase of rotor speed led to decrease of wind torque.

Optimal tip speed ratio of well-designed WT typically equals to 7–8 and depends mostly on design of blades. In case of used aerodynamic model, it equals to 8.1. Power output and optimal tip speed ratio curve for different wind and rotor speeds are presented in (Figure 4.4) on whole variable-speed range of the DFIG WT. It can be seen that maintaining optimal tip speed ratio leads to obtaining maximum power output, therefore it is a requirements for WT to follow optimal tip speed ratio on the variable-speed range.

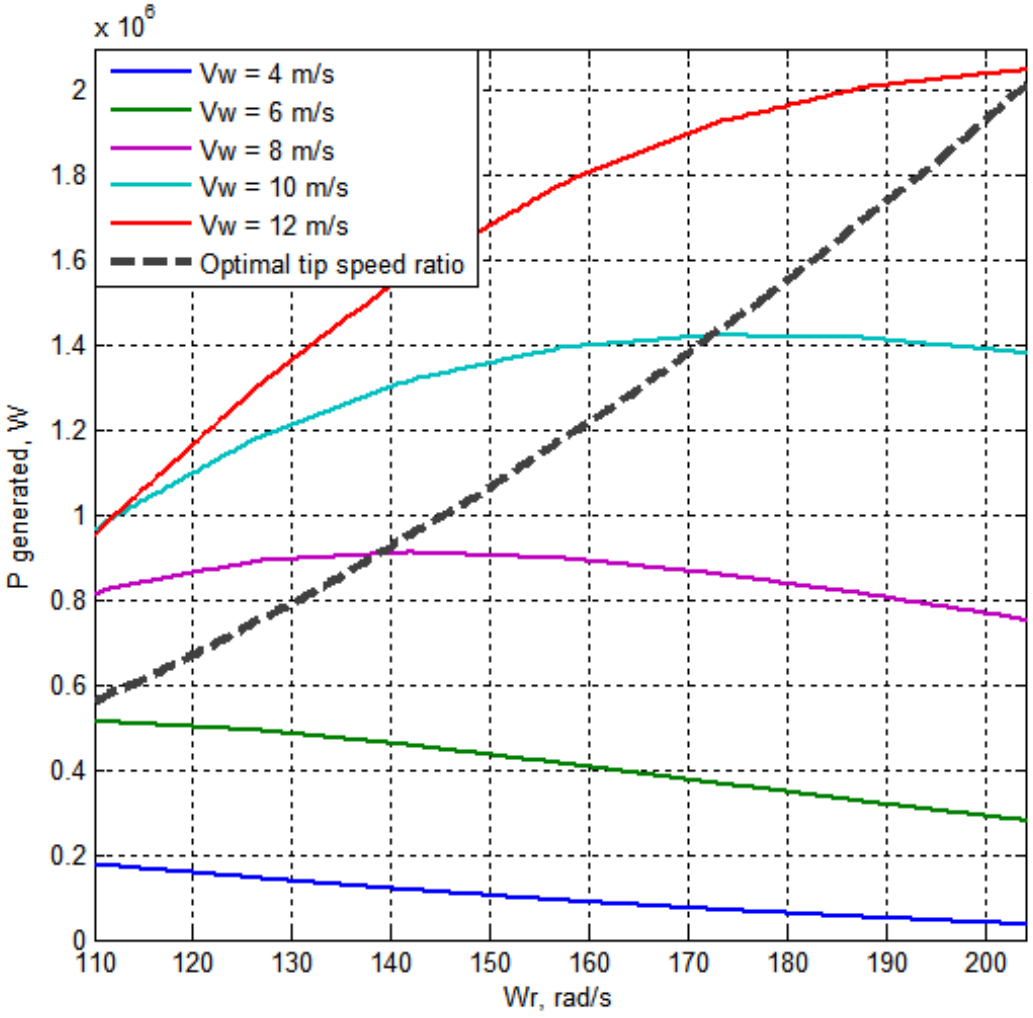

Figure 4.4. Possible power generated at different rotor and wind speeds.

Usually the wind speed is directly measure by the wind speed sensors placed on the WT. Considering (2.8) and the control law for optimal rotor speed on high-speed shaft may be written as follows:

$$\omega_r^{ref} = \lambda_{opt} v_w k_{dt} \quad (4.6)$$

Where k_{dt} is the drivetrain gear ratio.

However, there are control strategies that provide maximum power point tracking without wind speed sensors. In such case, the optimal tip speed ratio curve is represented as dependency of optimal rotor speed on produced power output, and predictive algorithms are used to find out the current position on optimal tip speed curve (Wang & Chang, 2004).

4.3 Operating at high wind speeds

While WT should produce rated power at rated wind speed, it also should normally operate on wind speeds higher than rated. In such conditions power applied to blades will be higher than rated and therefore power handled by both rotor and stator circuits will also exceed DFIG and power converter ratings. That situation may lead to reduced lifetime of the DFIG WT mechanical and electrical systems as well as to faults.

There are two ways to make WT possible to operate on high wind speeds – stall control and pitch angle control. Stall control is a design of rotor blades with special form, so at higher wind speeds they naturally reduce power captured from the wind. The advantage of stall control is that there is no need to control the power output. However, stall control leads to variable power output on high wind speeds, which is a serious disadvantage as a WT should be rated to peak power and therefore its efficiency will decrease around that peak.

4.3.1 Pitch angle control

The other way to provide high wind speeds operation is to use blades pitch angle control. According to this approach, rotor blades are connected to the hub via servo drives that can rotate blade around its axis, thus reducing the surface of wind facing. This approach is more expensive as blades are relatively heavy, but it allows to maintain constant rated power output on wind speeds higher than rated.

While blades pitch control is required only on wind speeds higher than rated, its control is usually based only on produced and delivered power to the grid as before its value the torque control should maintain necessary rotor speed. Pitch angle reference can be obtained according to next equations:

$$\beta = k_{PI}\left(P_{out} - P_{out}^{ref}\right) + k_{PI}\left(\omega_r - \omega_r^{ref}\right) \tag{4.7}$$

Where reference for power output P_{out}^{ref} is:

$$P_{out}^{ref} = \begin{cases} P_{out}, for\ P_{out} < P_{rated} \\ P_{rated}, for\ P_{out} > P_{rated} \end{cases} \tag{4.8}$$

And similarly rotor speed reference:

$$\omega_r^{ref} = \begin{cases} \omega_r, for\ \omega_r < \omega_{r\ rated} \\ \omega_{r\ rated}, for\ \omega_r > \omega_{r\ rated} \end{cases} \tag{4.9}$$

Such control guarantees absence of interference between the pitch angle and torque control, granting increased lifetime of mechanical parts, because torque control allows better handling of stresses, storing mechanical power variations in the form of electrical energy (Kulka, 2004).

4.3.2 Rotor speed margin

From the economical point of view rated output power should be achieved on the maximum slip value to minimize the power converter rating. At the same time, it provides maximum variation of rotor speed for lower wind speeds. However, in practice rated rotor speed is placed at 85-95% of the maximum negative slip value. When rated power output level is achieved, the pitch angle control has been enabled.

The purpose of rotor speed limitation in high-speed operating range is to create margin between the pitch angle control and torque control. Both pitch angle and rotor are inertial systems and if RSC runs out of current while blades speed still increases – pitch angle controller requires some

time to stabilize rotor speed. Through this time range, there will be spike in produced power with magnitude higher than rated, which leads to negative consequences for the DFIG WT system.

Hence, the buffer between torque control limitations and pitch angle control should exist and its value in per cents of rotor speed depends on rotor inertia and dynamics of the pitch angle control. Therefore, when pitch angle control is required, the rotor will already have stabilized speed. It is also should be noticed, that considering such rotor speed limitations, the rated power will be achieved not with optimal tip speed ratio and therefore rated power point will be placed lower on the [power/rotor speed] graph, which is shown in the Figure 4.4.

4.3.3 High wind speed operation

The simulation is carried out for wind speeds range 10–15 m/s to investigate the DFIG WT performance in a case when wind speed exceeds rated value 12 m/s. Results of simulation are shown in the Figure 4.5.

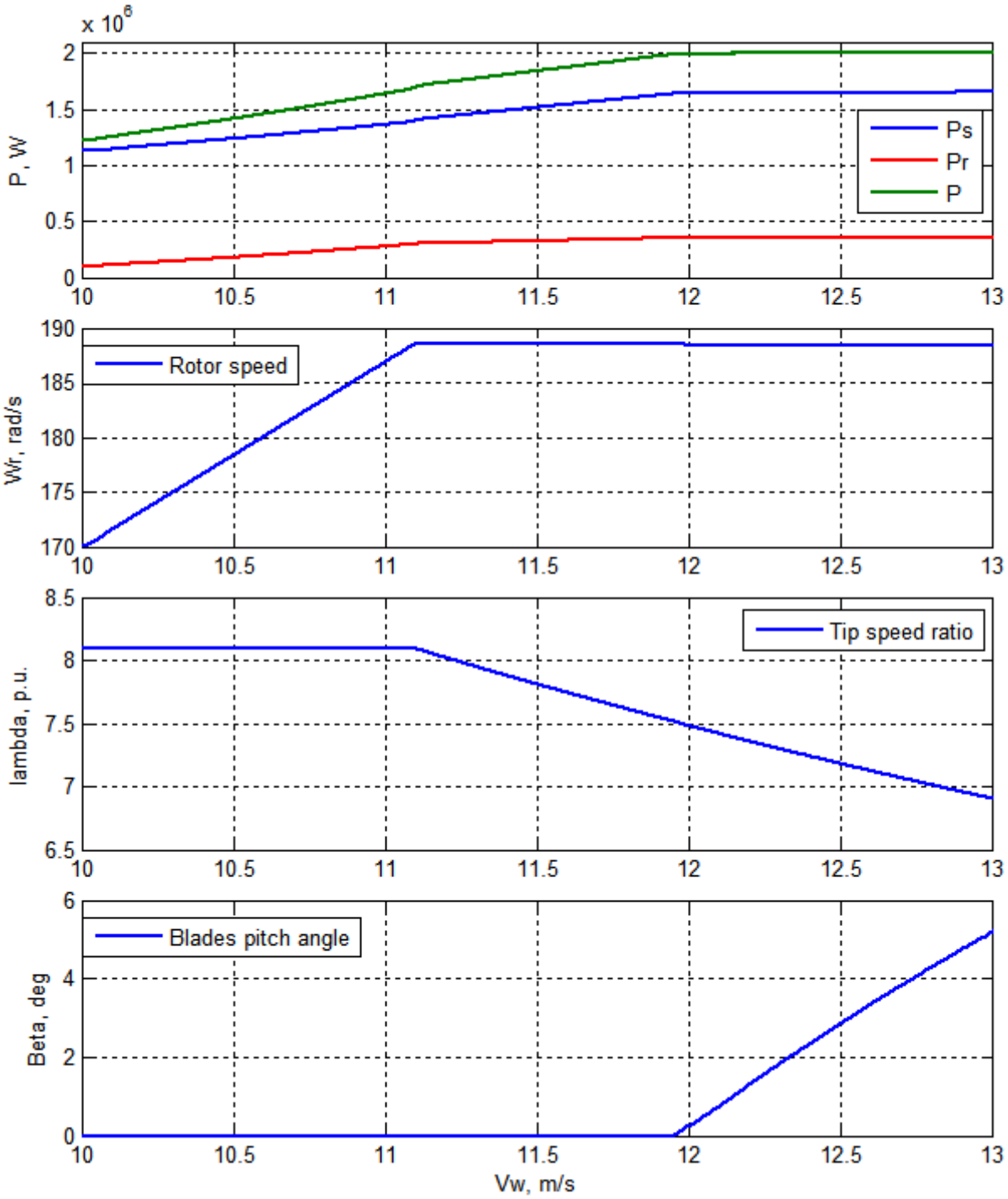

Figure 4.5. Higher wind speeds operation range.

4.4 Operation range of the DFIG WT

All described principles allowed to develop realistic operation range of the DFIG WT and develop a model suitable for operation under different wind speeds. Operation range of the DFIG WT is presented in the Figure 4.6. It consists of several points:

1. Point **A**. This is the point, where the DFIG WT connects to the grid and starts normal operation. Slip has maximum positive value 0.3. Produced power output is minimal. Below this point DFIG goes to motoring mode.

2. Segment **A–B**. Low wind speed operation. Rotor speed is constant at minimum value 110 rad/s to maintain maximum power output. Lower rotor speeds are impossible due to rotor voltage limitation. Tip speed ratio is above optimal.

3. Point **B**. WT reaches the optimal tip speed ratio. From this point variable-speed region begins.

4. Segment **B–C**. Variable-speed sub-synchronous operation. Up to 500 kW of generated power circulates in rotor circuit. Slip range: +0.3 → 0. Rotor speed range: 110–157 rad/s.

5. Point **C**. Synchronous operation. Slip equals to zero. Rotor power equals to zero. Output power equals to stator power. Synchronous rotor speed is 157 rad/s.

6. Segment **C–D**. Variable-speed super-synchronous operation. Up to 300 kW of generated power comes to grid through the rotor circuit. Slip range: 0 → –0.2. Rotor speed range: 157–188 rad/s. Tip speed ratio remains optimal.

7. Point **D**. Maximum reference rotor speed equaled to 188 rad/s. Variable-speed operation ends here.

8. Segment **D–E**. Torque control mode. Reference rotor speed keeps constant. Torque control uses current reserve to achieve rated power output. Tip speed ratio is below optimal.

9. Point **E**. Rated power output is achieved. Above this point, rotor speed and power is limited only by a pitch angle control as rotor current achieves its limit. This operation mode lasts until cut-off wind speed.

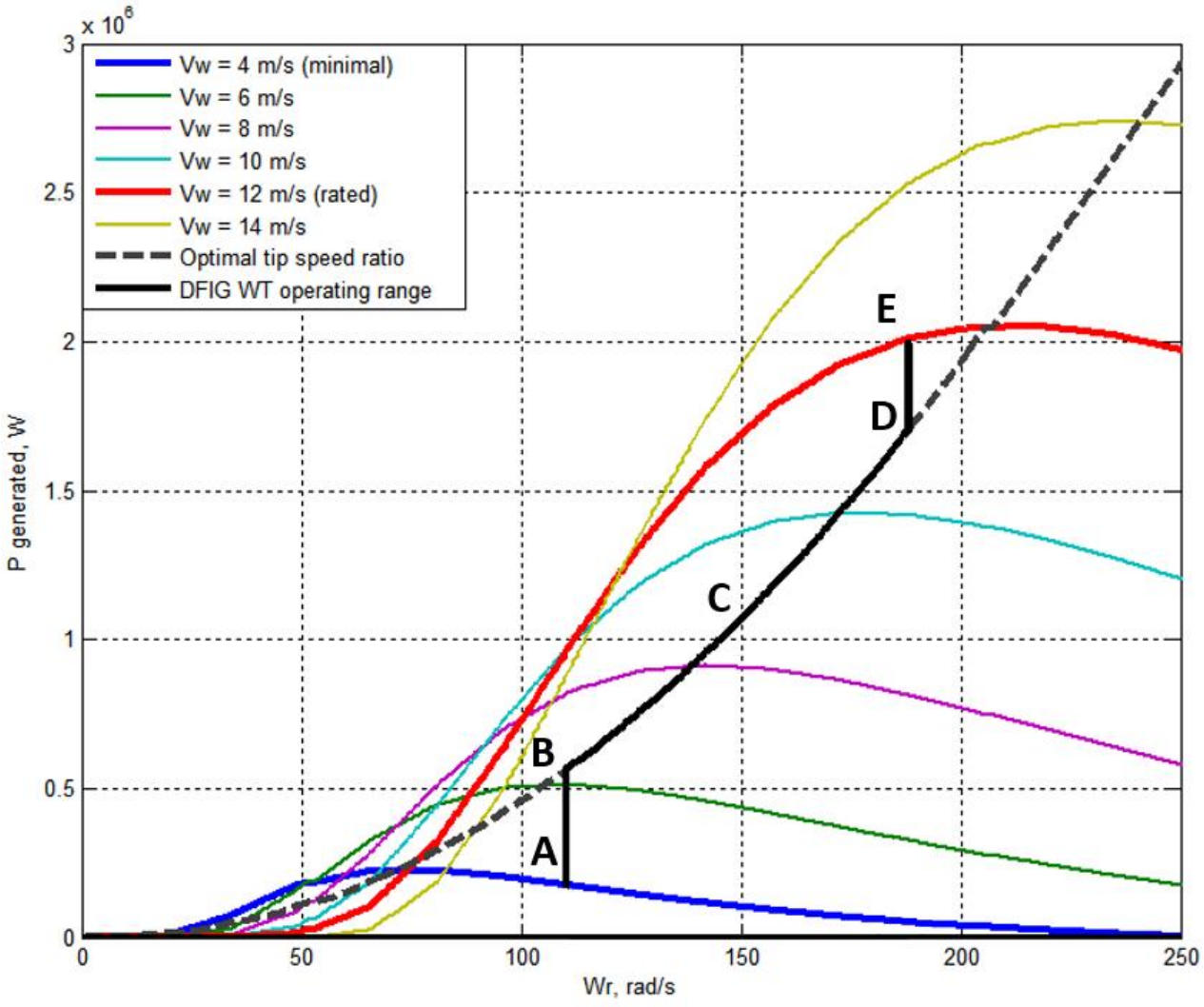

Figure 4.6. DFIG WT operation regions.

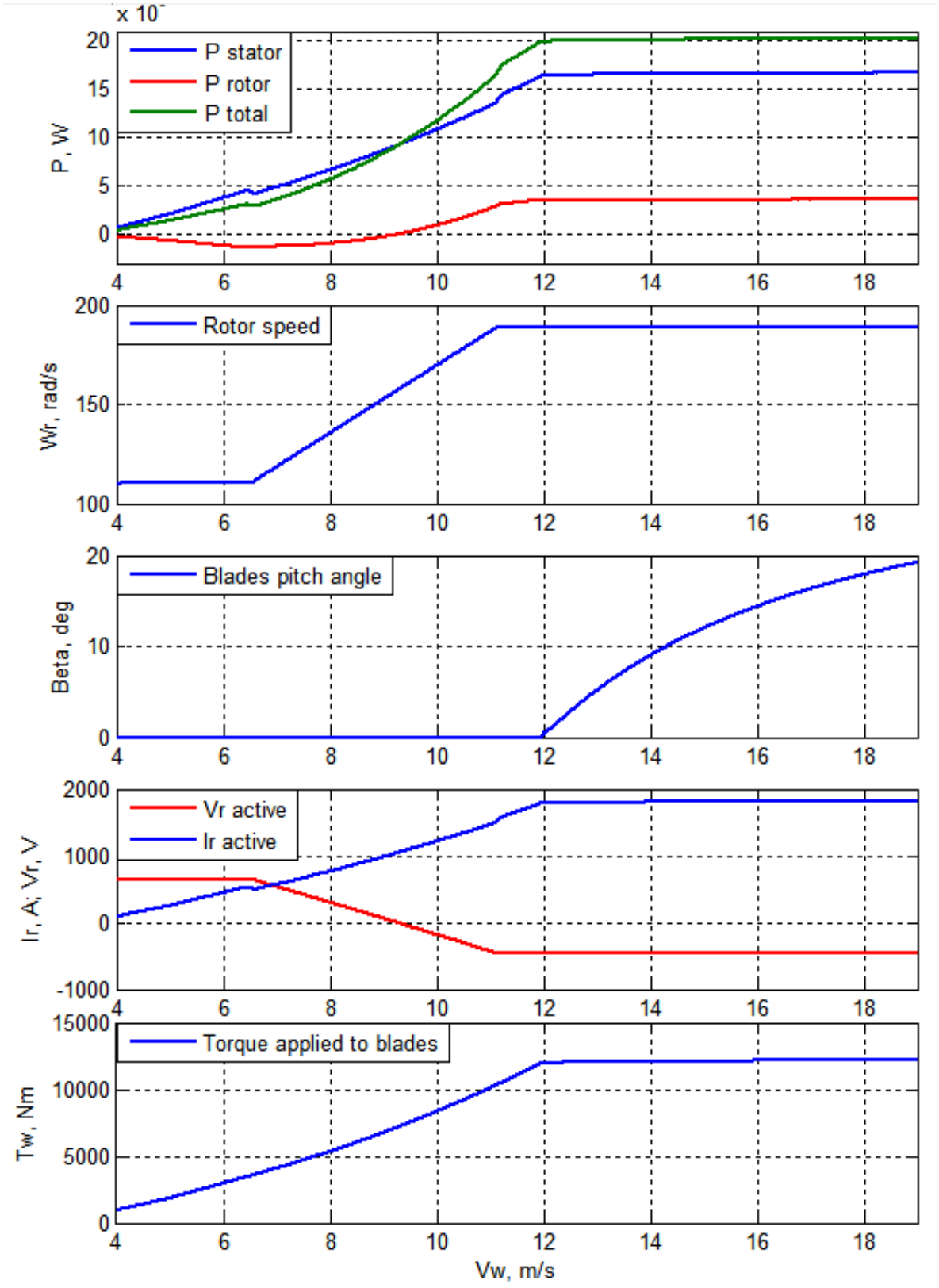

Figure 4.7. Aerodynamic model with optimal tip speed ratio illustrated.

To investigate DFIG WT behavior across entire operational region, the simulation was performed for wind speed range 4 – 20 m/s. Simulation results are shown in the Figure 4.7. Reference wind speed for aerodynamic model is generated as ramp starting from 4 m/s with slope 0.05 m/s. Despite very low slope, there are small traces of transition process in power output that would not exist in steady-state operation – decrease of power output when rotor starts to accelerate (7–11 m/s range).

It can be seen from the figure that DFIG WT model clearly follows operation range described above.

1. 4–6.5 m/s. **A–B** range.
2. 6.5–9 m/s. **B–C** range.
3. 9–11 m/s. **C–D** range.
4. 11–12 m/s. **D-E** range.
5. 12–20 m/s. **E+** range.

4.5 Dynamic analysis

While previous simulations mainly consider steady-state operation of the DFIG WT, this section contains investigation of the DFIG WT dynamic behavior. Simulation of DFIG WT dynamic response is made by generating random wind speeds profile as input for aerodynamic model.

There are different ways to simulate wind speeds distribution described in literature. Some of them are complex and take a landscape data to provide realistic wind distribution for a wind farm. However, in our case, the much more simplified model can be used, because of investigation of only one WT behavior. For the generating of wind speeds applied to single WT and in the lack of any specific data, stochastic models based on normal distribution, Weibull distribution, autoregressive models or Markov chains can be used (Burton, Jenkins, Sharpe, & Bossanyi, 2011).

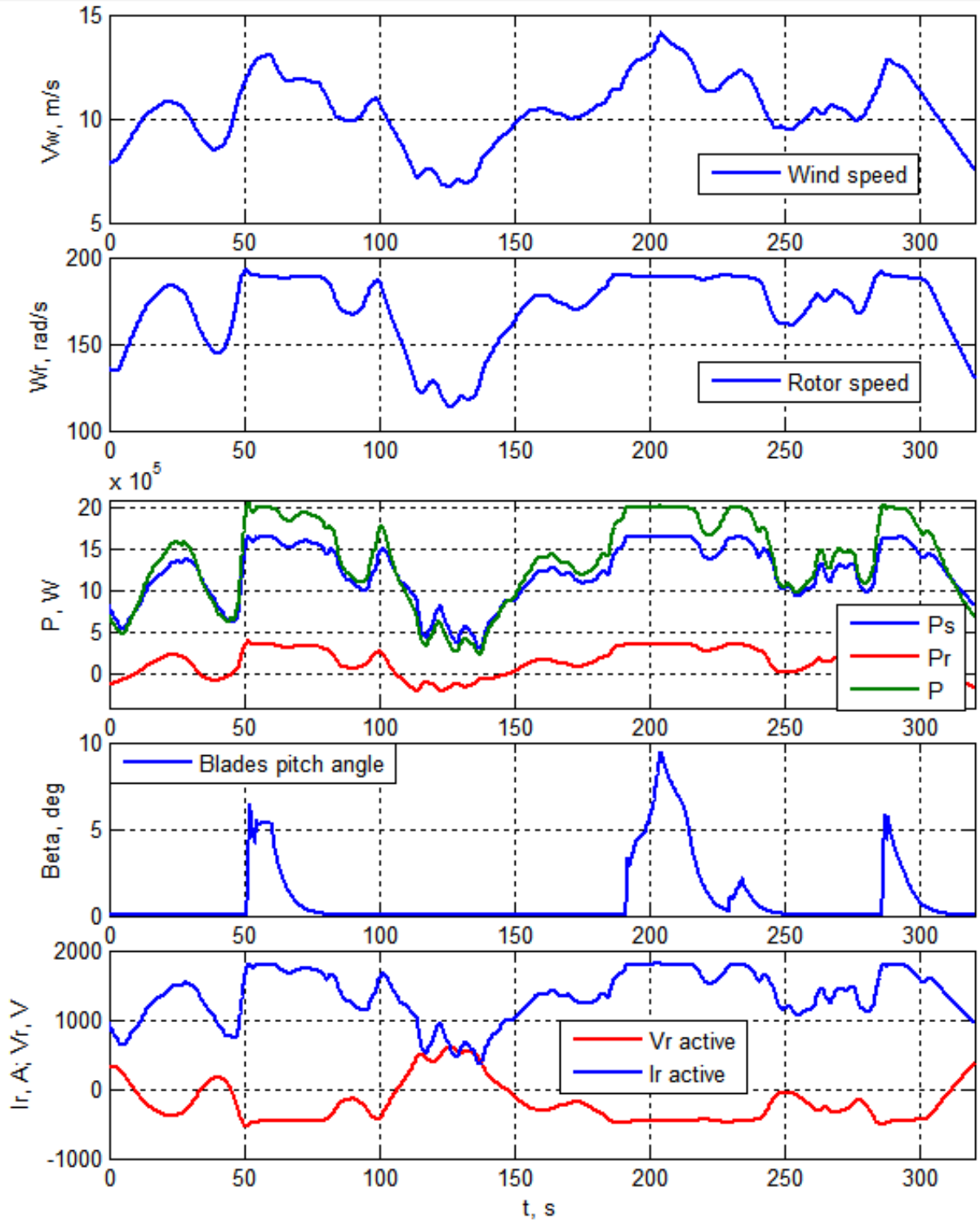

Figure 4.8. Simulation of DFIG WT dynamic behavior.

Dynamic wind behavior in this work was modelled as random generated sequence of the wind speeds with normal distribution parameters. Average wind speed was chosen to be 10 m/s and normal variance to be 5 m/s. Matlab *randn* function was used to generate normally distributed sequence of the 300 wind speed values. Then the sequence was smoothed with using a moving average filter by Matlab *smooth* function. Produced wind speeds set was interpolated on a 300 seconds range and was used as input for the aerodynamic model.

Results of simulation are shown in the Figure 4.8. It can be seen how all principles implemented in model and described throughout the thesis work in real-time. On the higher wind speeds pitch angle control limits power and rotor speed keeps its maximum value. On the variable-speed range, rotor speed tracks the wind speed to maintain optimal tip speed ratio.

5 Reactive power control of the DFIG WT

5.1 Reactive power capabilities

5.1.1 Reactive power flow in rotor circuit

Normal DFIG WT variable-speed operation requires not only active current flow in the rotor circuit to produce torque and therefore control rotor speed. Maintaining rotating magnetic field also requires some magnetizing current, which determines reactive power flow that should be provided by RSC.

Necessity to provide reactive power flow in rotor circuit affects the RSC power rating. RSC current rating therefore should be chosen not only according to active current, which was assumed in previous chapter, but also should consider necessary reactive current component. SFO control system allows to naturally decouple rotor current components in active i_q, which determines torque generation capabilities, and reactive i_d, which is required to provide magnetizing reactive power flow and ability to control stator reactive power. Overall current rating in synchronous reference frame is defined as rotor current magnitude:

$$i_{rated} = \sqrt{i_{d\_rated}^2 + i_{q\_rated}^2} \tag{5.1}$$

Achievement of q-axis component is presented in chapter 4. Equation (3.1) shows that magnetization current is already considered in reference reactive current generation. Therefore, reactive current reference relates only to stator reactive power generation. Reactive power flow required only for magnetization therefore is investigated with providing reactive current reference as:

$$i_d^{ref} = 0 \tag{5.2}$$

Simulation of the DFIG WT operation on variable-speed range was implemented with zero reactive current reference. The Figure 5.1 shows distribution of reactive power in the DFIG WT electrical circuits while reference reactive current for RSC control system remains zero. It can be seen that for proper operation DFIG rotor consumes reactive power from RSC at sub-

synchronous speed range and supplies reactive power on super-synchronous speeds similarly to active power flow through the rotor.

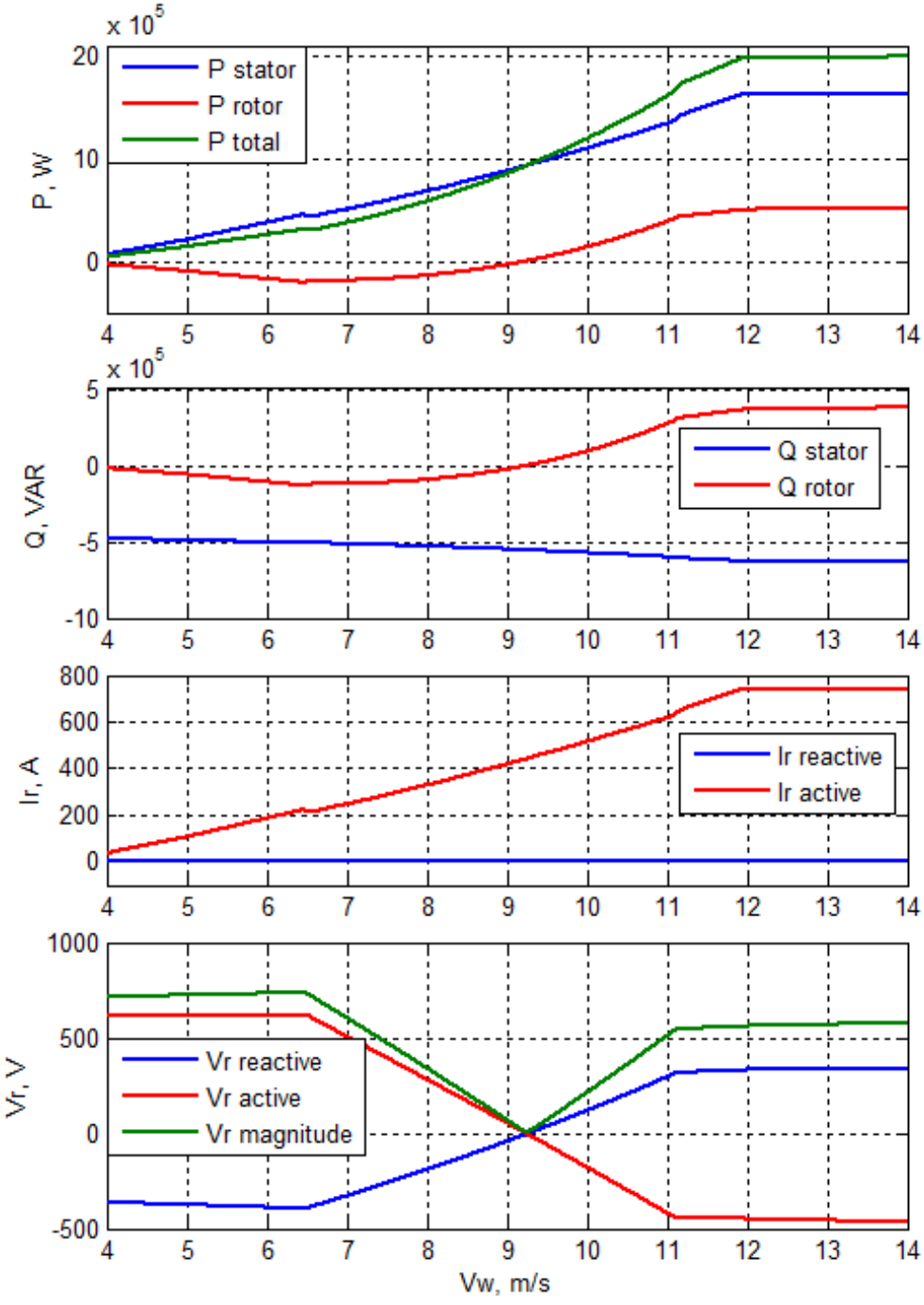

Figure 5.1. Simulation results: reactive power flow in variable-speed operation.

Results also show that while rotor active power counter-follows rotor voltage active component v_q, reactive power follows reactive voltage component v_d. Opposite signs of voltages active and reactive components are explained by orientation of *d*-axis along the stator flux vector. It also can be observed that voltage rating of power converter also depends on both active and

reactive voltage components, which should be considered in converter design. Similarly to active voltage component v_q, v_d determines mostly not the possible amount of generated reactive power, but maximum slip values at which reactive power may be generated. Rotor reactive power does not affect power exchange with grid because of back-to-back power converter topology natural ability to decouple reactive power.

It also should be noticed that if RSC does not control reactive current, DFIG stator consumes reactive power from the grid. This is explained by the fact that any induction motor or generator requires source of magnetizing current to maintain lagging magnetic field. In standalone operation, magnetizing current is provided by capacitors bank placed in parallel at IG terminals, while in grid-connected operation IG consumes excitation currents from the grid. Figure 5.1 shows that reactive power absorbed by stator follows increase of generated active power, which is because of required excitation currents are determined by generator power factor and therefore it is a fraction of the apparent power.

5.1.2 Reactive power capabilities at variable-speed range

While chapter 4 presented choice of RSC current rating according only to active power flow in rotor circuit, the magnetizing current was also considered as it is required to provide DFIG operation. It is clear that DFIG WT with converter rated for providing only normal operation cannot be a good source of reactive power as it strikes the current limitation. However, as it was shown in previous chapter, current load significantly decreases at low wind speeds as mechanical power becomes lower, therefore it is useful to investigate reactive power capabilities of the DFIG WT rated for only active power generation at variable speed range.

As maximum current magnitude possibly handled by RSC is set to rated active current, we can investigate reactive power capabilities of the DFIG applying reactive reference current as free current reserve of RSC. Reference reactive current is then calculated according to:

$$i_d^{ref} = \pm\sqrt{i_{rated}^2 - \left(i_q^{ref}\right)^2} \tag{5.3}$$

Simulation was made by applying both positive (capacitive operation) and negative (inductive operation) reactive current reference on the variable-speed range. The simulation results are presented in Figure 5.2. Results show that reactive power generated by stator clearly follows i_d component, which value depends on available current of RSC and is in reverse ratio to active current presented in Figure 5.1, as current magnitude remains constant at rated value.

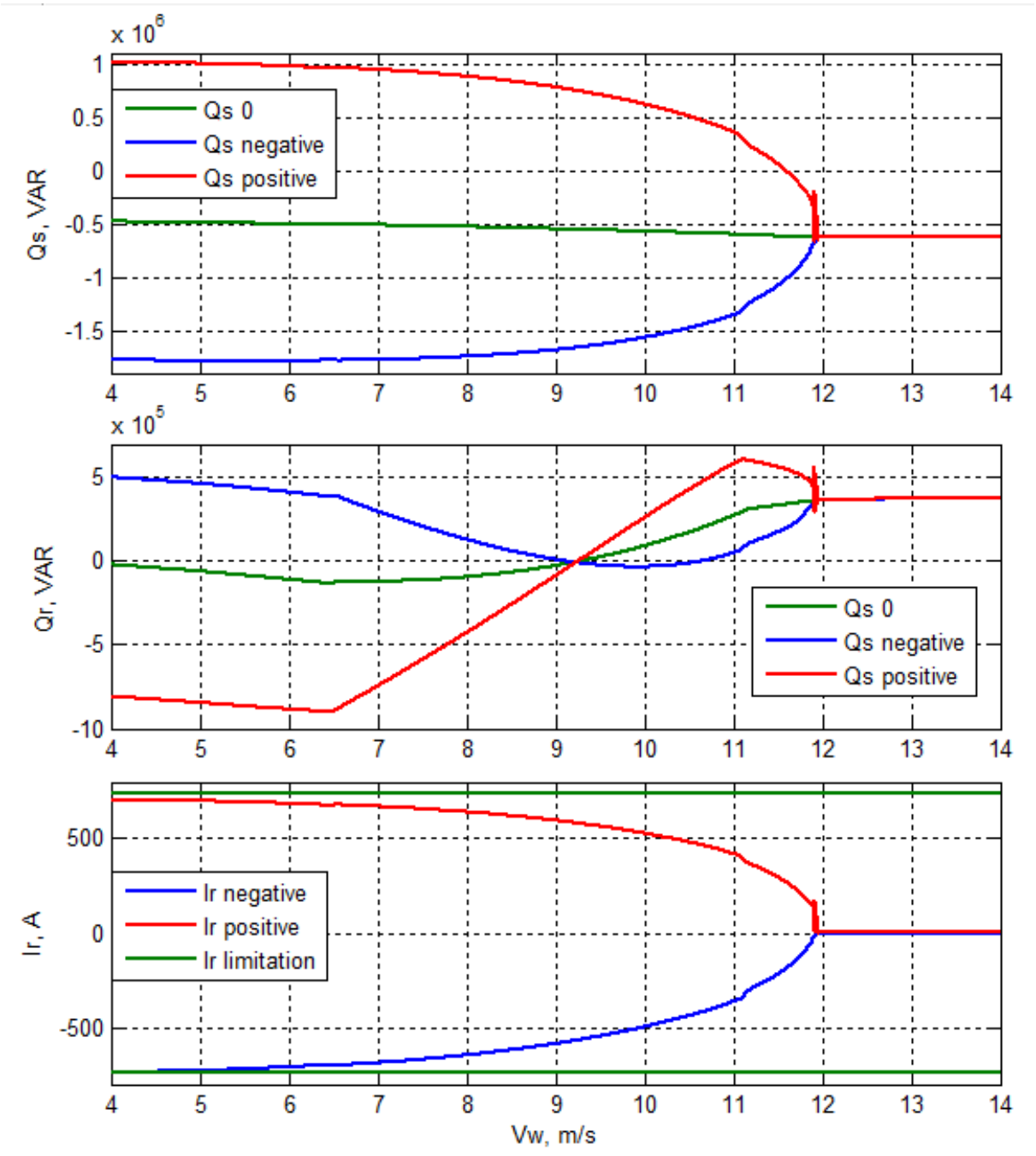

Figure 5.2. Simulation results: reactive power capabilities in variable-speed operation.

As active current achieves RSC current magnitude limitation at rated wind speed (12 m/s), reactive power control abilities become zero, and both capacitive and inductive operation curves of stator reactive power become joined at stator magnetizing reactive power value.

5.2 Power factor correction

5.2.1 Fingrid requirements for power factor correction

The first major requirement stated by FinGrid is the ability to maintain specific values of power factor at different voltage levels. Requirements for the reactive power capabilities of wind power applications rated for 1–10 MW are shown in diagram (Figure 5.3). The wind power plant of such rate should be able to:

- Maintain 0.995 inductive power factor (overexcited), when the network voltage is in the range 90-100%.
- Maintain 0.995 capacitive power factor when the network voltage is in the range 100-105%.

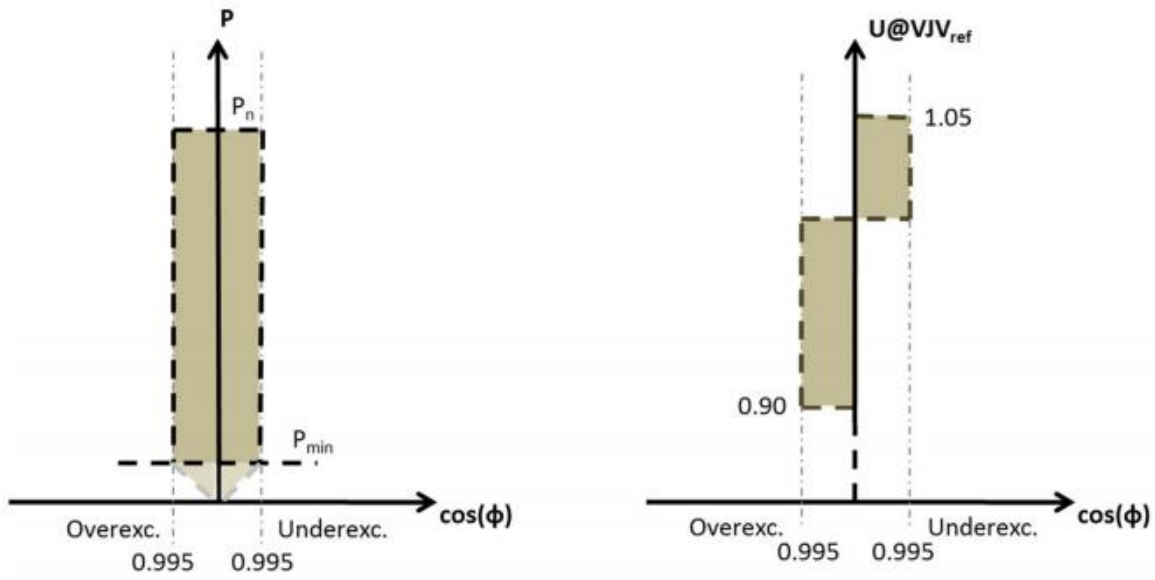

Figure 5.3. Requirements for power factor stated by Finnish grid codes. (Fingrid's grid code requirements set for wind power plants has been updated, 2015)

Reactive power capacity is expressed in terms of power coefficient as follows:

$$sin\phi = \sqrt{1 - \cos^2 \phi}$$
$$Q = sin\phi |S| \tag{4.4}$$

For required 0.995 power factor reactive power injected by the WT to the grid can be rewritten as follows:

$$Q = \pm\sqrt{1 - 0.995^2} \cdot |S| \approx \pm 10\% \cdot P_{rated} \tag{4.5}$$

According to entire operating range of the DFIG WT we consider maximal power as rated power equals to 2 MW and minimal power as total power at the minimal wind speed 4 m/s equals to 50 kW. Therefore, $Q_{max} = \pm 200$ kVar.

5.2.2 Under- and overvoltage operation

As grid codes state requirements for power control on different grid voltage levels, it is necessary first to investigate reactive power capabilities of the DFIG WT in under- and overvoltage conditions. Simulations similar to made in section 5.1.2 were carried for three voltages levels: 90%, 100% and 105% of nominal grid magnitude 10 kV.

Results of simulations are shown in Figure 5.4 with plotted power factor requirements. The Figure 5.4 shows that grid voltage level directly affects reactive power capabilities of the DFIG WT – lower grid voltage levels reduce reactive power capabilities of the WT, while overvoltage in contrary enhances ability to control stator reactive power.

Interconnection of the grid voltage level and reactive power capabilities is explained as follows. Grid voltage is directly coupled voltage levels in both stator and rotor circuits because of three-winding transformer connection. As both active and reactive powers are product of current times voltage corresponding components, increased voltage levels provide higher power for

actual current rating. Ability to operate in 90–105% voltage range should be considered in the voltage ratings when designing both power converter and DFIG.

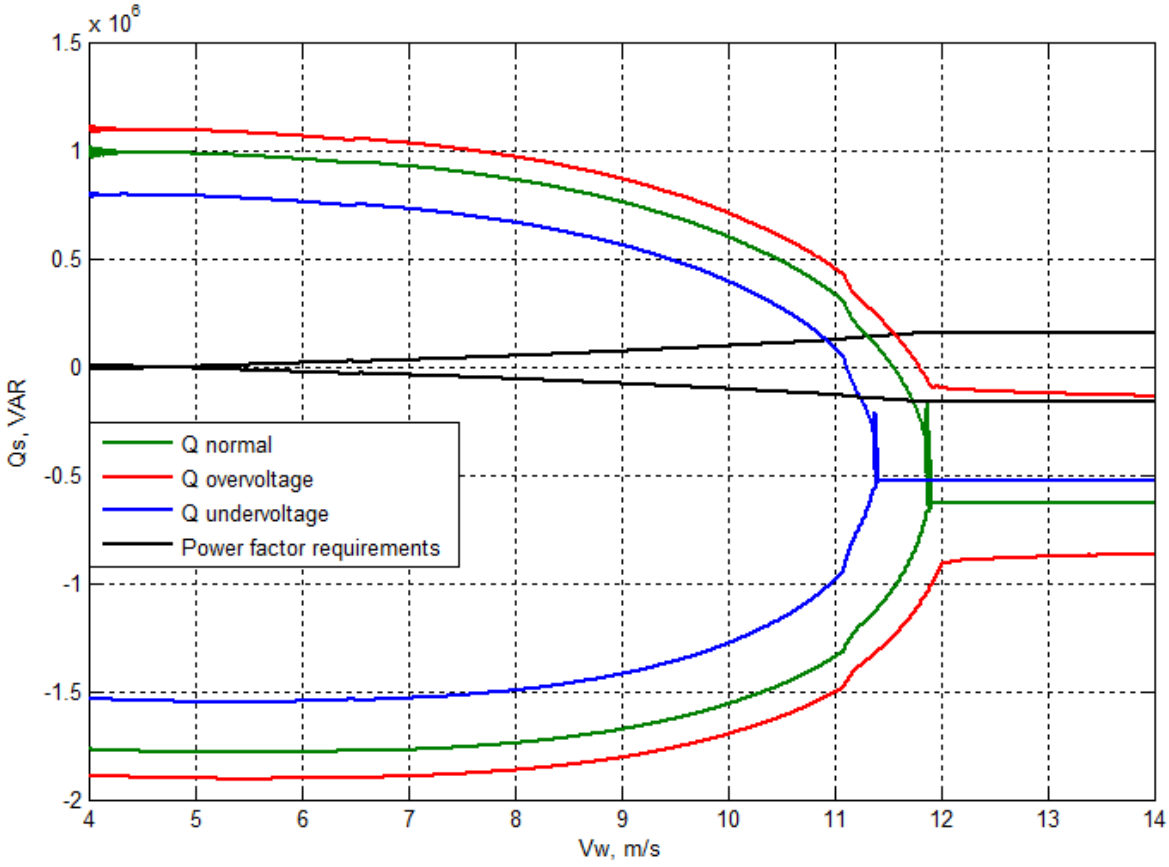

Figure 5.4. Simulation results: DFIG WT reactive power capabilities in normal, under- and overvoltage grid conditions.

5.2.3 Fulfillment of power factor requirements

Results of different grid voltages conditions simulation (Figure 5.4) show that the most intense and therefore challenging operating mode of the DFIG WT is undervoltage operation. At grid voltage levels below nominal, the RSC requires more current to produce the same reactive power output as in rated voltage conditions. Therefore, current rating of rotor power converter should be chosen for minimal FinGrid voltage level requirement – 90% of nominal.

Simulation of the DFIG WT in PLECS allows knowing exactly how much current does need the RSC to maintain necessary power factor in any grid conditions. As RSC control system has reactive power controller, which is described in section 3.1, maximum current vector magnitude

for RSC can be achieved by applying reactive power reference to RSC control system according to (5.5) and limiting only active current at rated value, obtained in chapter 4 (740 A).

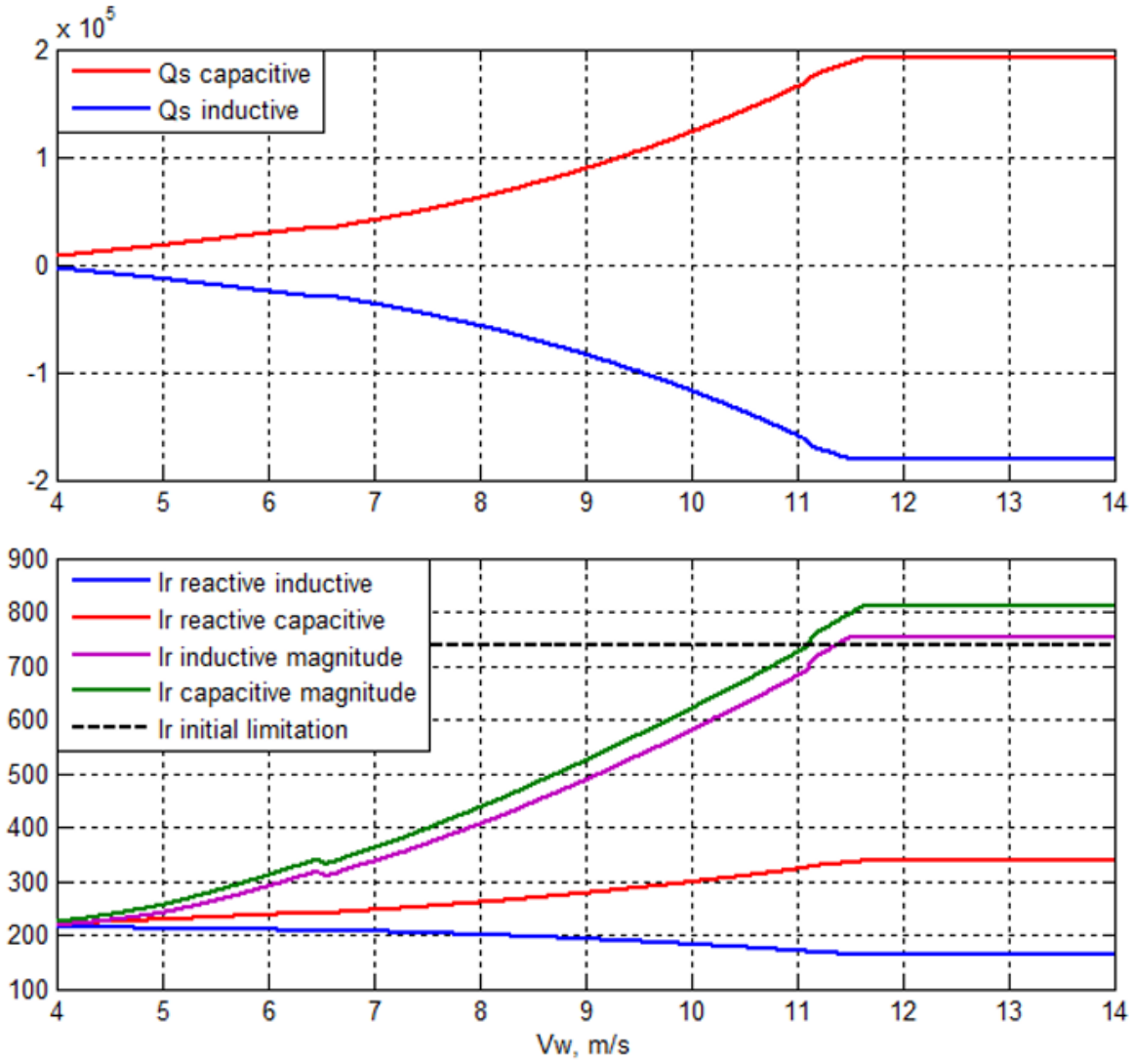

Figure 5.5. Simulation results: Current rating required for providing necessary power factor in undervoltage conditions.

Simulation results for such conditions are presented in Figure 5.5. The description of curves:

- *Qs capacitive* – reactive power in capacitive operation mode, WT generates reactive power to the grid; *Qs inductive* – reactive power in inductive operation mode, WT absorbs reactive power from the grid.
- *Ir reactive inductive* – value of reactive rotor side current i_{rd} when WT is in inductive operation mode; *Ir reactive capacitive* – value of reactive rotor side current i_{rd} when WT is in capacitive operation mode.

- *Ir inductive magnitude* – magnitude of rotor side current $|i_r|$ when WT is in inductive operation mode; *Ir capacitive magnitude* – magnitude of rotor side current $|i_r|$ when WT is in capacitive operation mode.
- *Ir initial limitation* – limitation of rotor side current magnitude $|i_r|$ achieved in previous chapter.

It can be seen that the largest value of current is required to provide necessary capacitive operation (+200 kVAR on rated wind speed) in undervoltage conditions. RSC current rating therefore is chosen to achieve the capacitive operation and equals to 810 A. It should be noticed that only RSC requires increase of current rating by 70 A, as reactive current only exists between the RSC and DFIG rotor.

5.2.4 Reactive power capabilities of DFIG WT rated for power factor correction

To verify that RSC current rating was chosen properly, the simulation of reactive power capabilities for DFIG WT with rated RSC was performed. Results of simulation are shown in Figure 5.6 for undervoltage and normal operation of the WT.

The simulation results show that current rating of the RSC set according to previous simulation allowed DFIG WT to maintain required capacitive power factor at rated wind speed and undervoltage grid conditions. DFIG WT therefore can provide reactive power control from 200 kVAR of capacitive operation to –1.2 MVAR of inductive operation at rated wind speed.

However, it also can be noticed from Figure 5.6 that at low wind speeds high capacitive current reference lead to variations of generated reactive power. That is explained by close approaching to voltage limitation of RSC, where a lot of reactive power required and active power at the same time remains low. Unstable behavior in such conditions is a well-known issue of the vector control systems. (Cartwrigh, 2006). To avoid that problem reactive current reference should be limited to maximum value, that allows stable operation, which is also shown in simulation results. The other solution may be using DTC or DPC strategies for RSC control algorithm as they provide more stable operation.

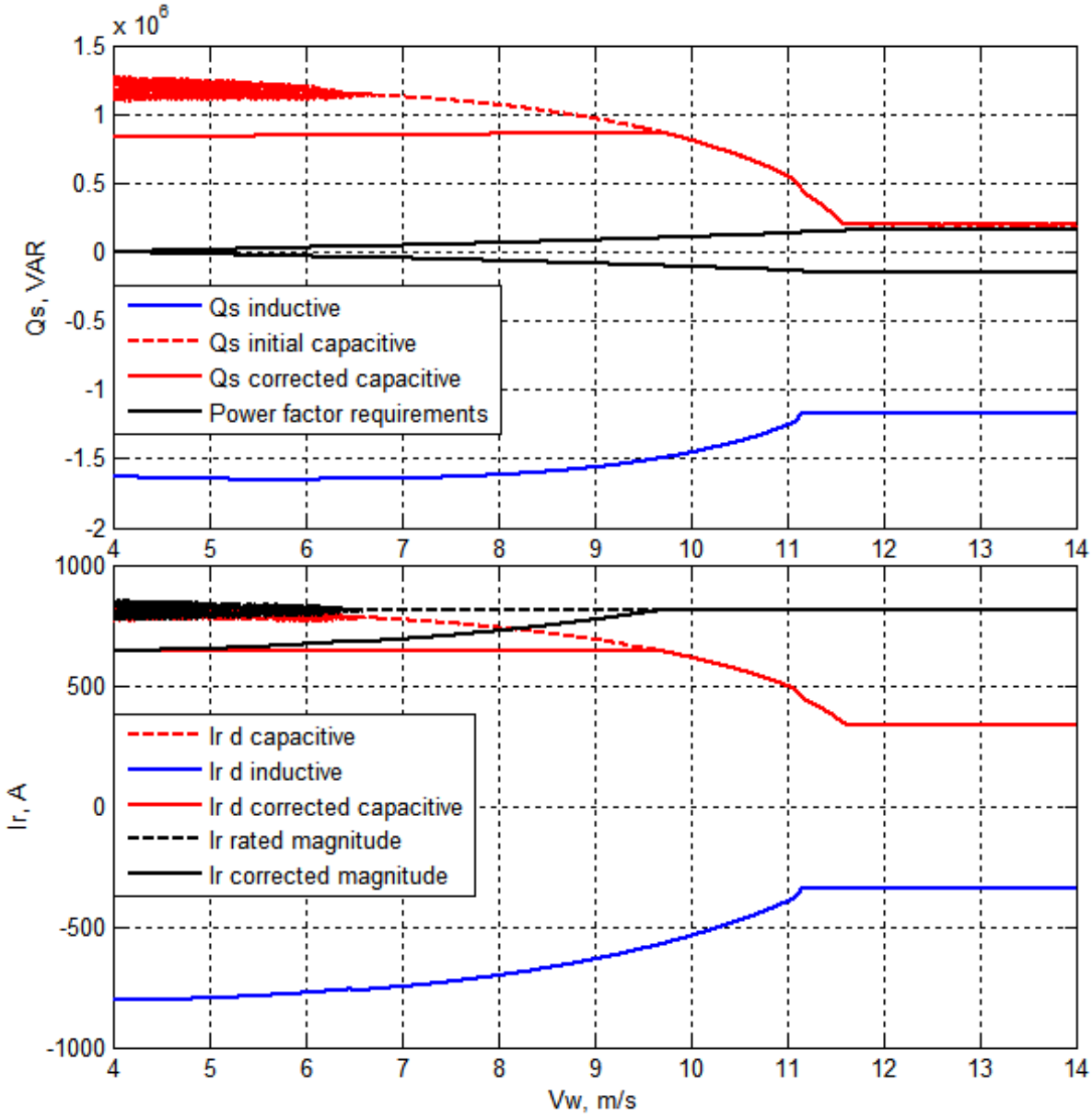

Figure 5.6. Simulation results: Reactive power capabilities of DFIG WT rated for power factor correction.

5.2.5 GSC reactive power capabilities

In the DFIG WT system, GSC can be also used to generate or absorb reactive power from the grid. However, GSC ability to control reactive power clearly follows the same ability of the RSC, because of they share the same amount of active power. To investigate reactive power capabilities of GSC the simulation was made with generating reference reactive current for GSC according in the same way as it was made for RSC – according to equation 5.1.

Results of simulation are presented in Figure 5.7. The figure shows that GSC can generate up to ±400 kVAR of reactive power, however only on wind speeds below rated, as the converter is not heavy loaded with active current.

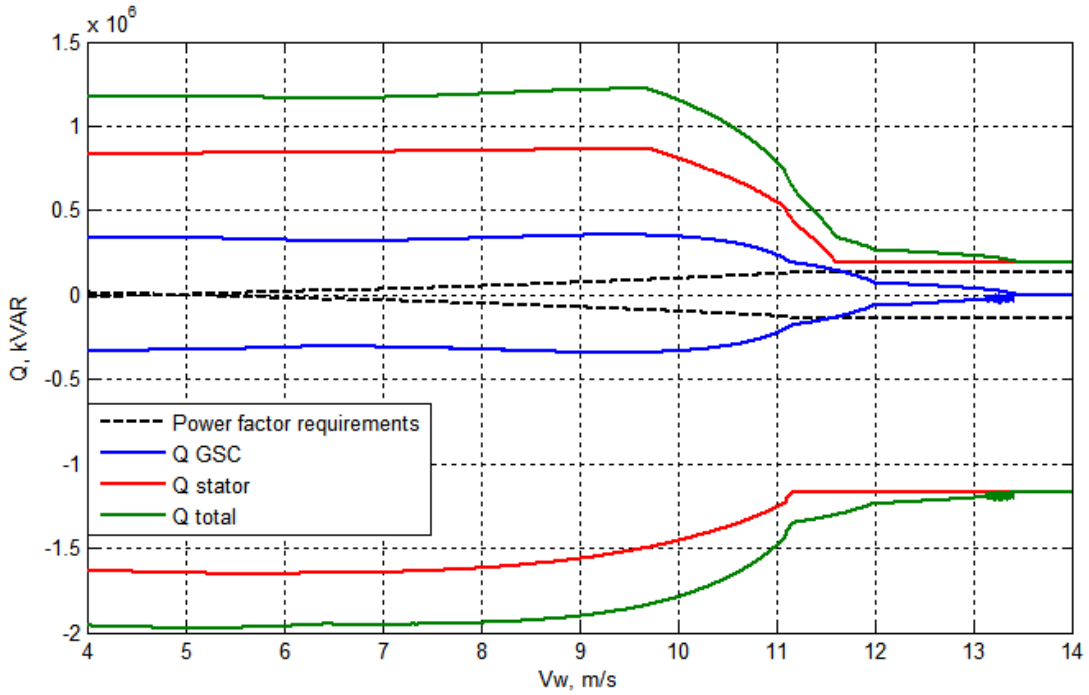

Figure 5.7. Simulation results: Reactive power capabilities of GSC.

5.3 Grid fault response

Disconnection of the WT from the grid during short grid faults leads to lack of power generation as resume of WT operation takes a time. Therefore, transmission system operators claim some special voltage sags waveforms, which WTs connected to the grid must be able to survive without being disconnected from the grid. Voltage sag waveform of Fingrid requirements is presented in the Figure 5.8.

Results of voltage sag simulation are presented in Figure 5.9. Figure shows that on 10 second of simulation grid voltage magnitude drops to 25% level. Torque control is based on maintaining necessary flux, and flux in order depends on grid voltage. When grid voltage drops, DFIG flux also drops and RSC cannot maintain necessary rotor speed anymore, which leads to

its increase. However, pitch angle controller also reacts on excessive rotor speed and limits it with increase of blades pitch angle.

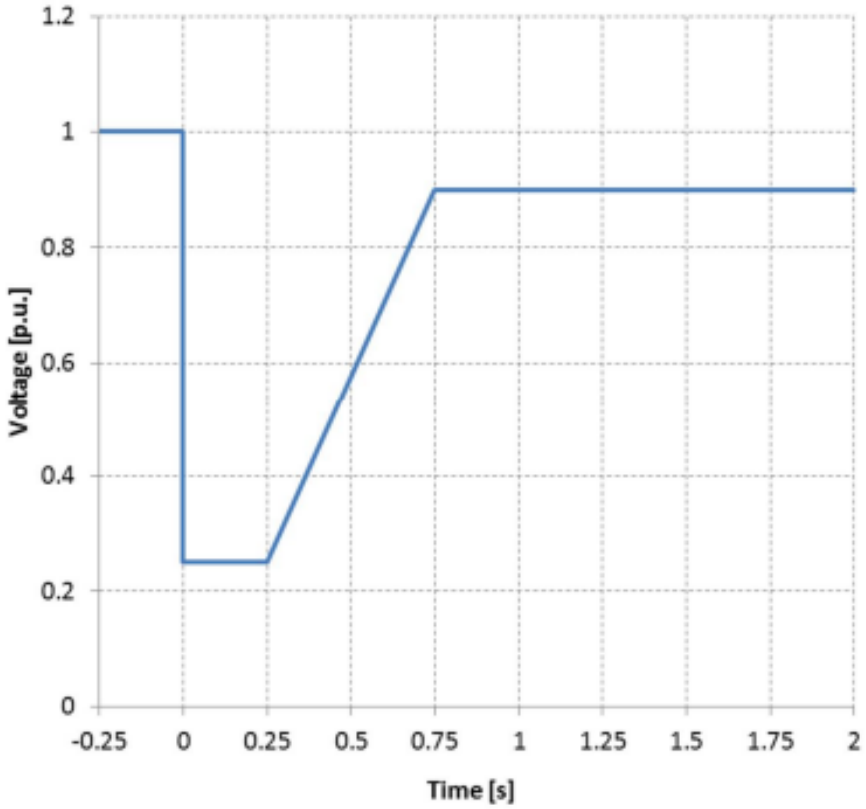

Figure 5.8. Reactive power capabilities of GSC. (Fingrid's grid code requirements set for wind power plants has been updated, 2015)

During the fault, GSC cannot deliver stored power to the grid and it leads to overvoltage of the DC-link. To prevent overvoltage the shunting resistor is continuously turned on (10–12s) and dissipates excess of DC-link power as heat energy. During the overvoltage, DC-link controller integral gain saturates and when grid voltage comes to normal value, GSC transfers more active power to the grid, than it is required, so DC-link voltage drop follows grid voltage restoration. However, after DC-link voltage drop control comes to normal operation.

As grid fault is followed by undervoltage, at that operation RSC cannot maintain enough torque to produce rated power, as it runs out of current. Therefore, to prevent increase of rotor speed, pitch angle controller keeps blades angle at value of 2 degrees and generated power in undervoltage conditions is 1.8 MW at rated speed instead of 2 MW.

Simulation shows that developed DFIG WT model can easily survive such faults without disconnection from the grid.

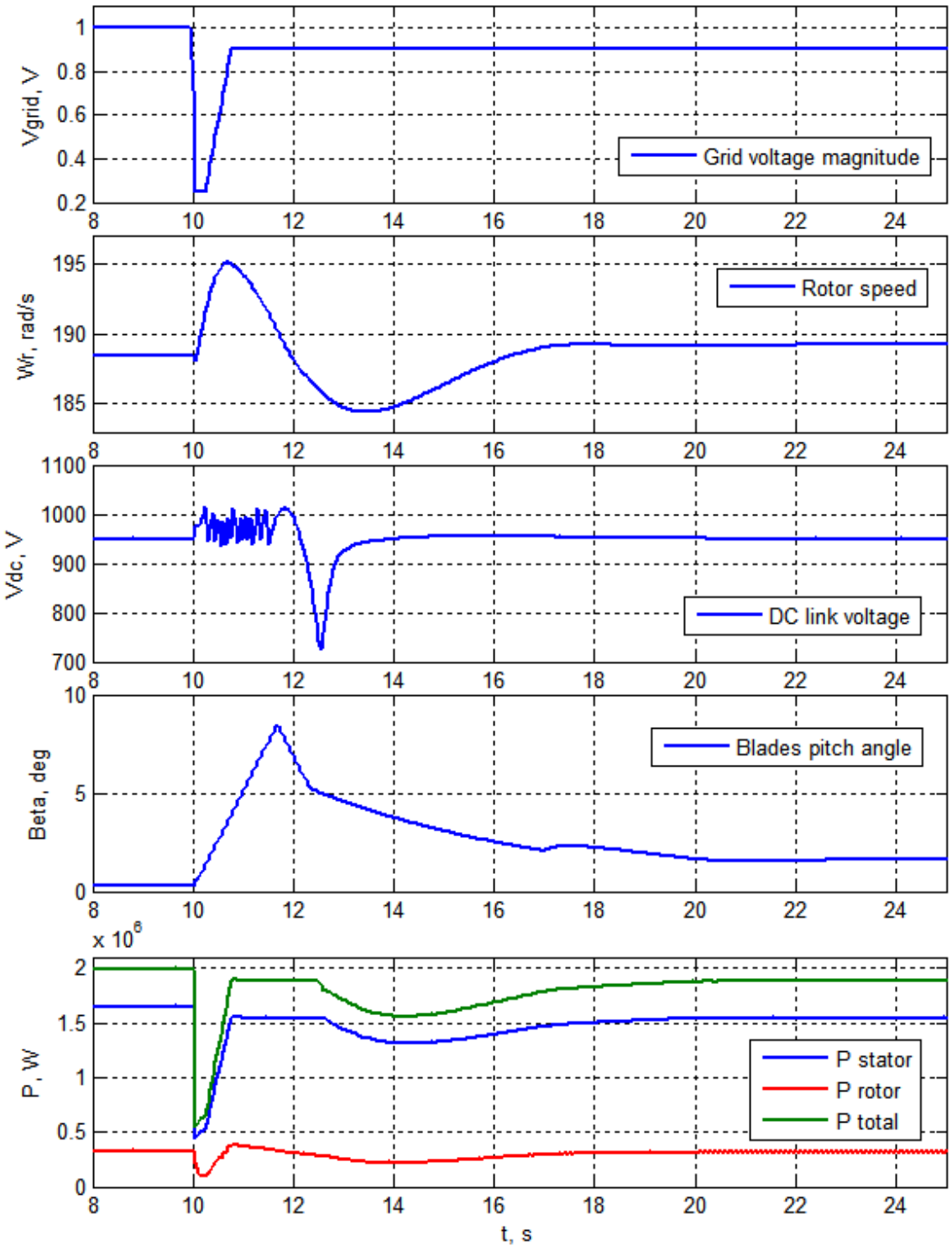

Figure 5.9. Simulation results: Reactive power capabilities of GSC.

5.4 Voltage regulation

Developed rated WT has enough reactive power capabilities on rated wind speeds to maintain 0.995 power factor correction and a lot more reactive power reserve on lower wind speeds. One of the main possibilities to use that power is to provide necessary voltage level.

As grid voltages in real grids may deviate, it is a useful ability for wind farm to maintain that voltage level at appropriate levels without additional equipment. From the control point of view it means that reference reactive power for reactive power controller, which is described in equation 3.1, should be assigned according to grid voltage level. However, reactive power in equation 3.1 can be replaced by stator voltage magnitude if we neglect stator resistance.

Therefore, reactive current reference becomes:

$$i_{di}^{ref} = K_{PI}(V_{grid}^{ref} - V_{grid}) \tag{3.32}$$

As it was described above, reactive current reference should be limited according to capabilities of the DFIG WT, as it may lead to instability of vector control system. Produced reactive current reference therefore limited by free current magnitude (3.1) and capacitive current also always limited to value, obtained in 5.2 – 600 A.

Investigation of dynamic behavior of the DFIG WT with grid voltage controller was made for the case of wind speed variations similar to section 4.8 with simultaneous grid voltage variations. Results of the simulation are shown in the Figure 5.10.

There are several conclusion, which can be made from the Figure 5.10. It can be seen that when voltage at DFIG WT terminals deviates from the nominal value, grid voltage controller generated reactive power reference to compensate voltage variations, so when voltage is lower than nominal, reactive power is generated to the grid, while when voltage is higher – DFIG WT absorbs reactive power.

It can also be noted that both GSC and RSC are involved in voltage stabilization, however GSC reactive power capabilities are lower than DFIG. That is because RSC was designed to provide power factor correction, while GSC was designed only to provide active power for proper RSC work, so its current rating is lower.

Grid voltage controller uses only free current of RSC to prevent the reduction of active power generation. Limited reactive power generation is clearly seen in 180–200 seconds of simulation, where increase of active power generation until nominal value accompanied with reduction of reactive power absorbed from the grid.

However, overall results of voltage stabilization show that properly designed DFIG WT can be used for voltage stabilization at terminals, as in proposed simulation DFIG WT rated to provide 0.995 power factor reduces average voltage deviation from 7.5% to 3.2%.

Another observation is that active power generation also affects voltage level. Green line shows voltage level on substation which is supposed to be connected via 20 km cable line to the WT substation. While cable line provide some voltage losses, it can be seen, that voltage at the DFIG WT terminals is higher than in the grid.

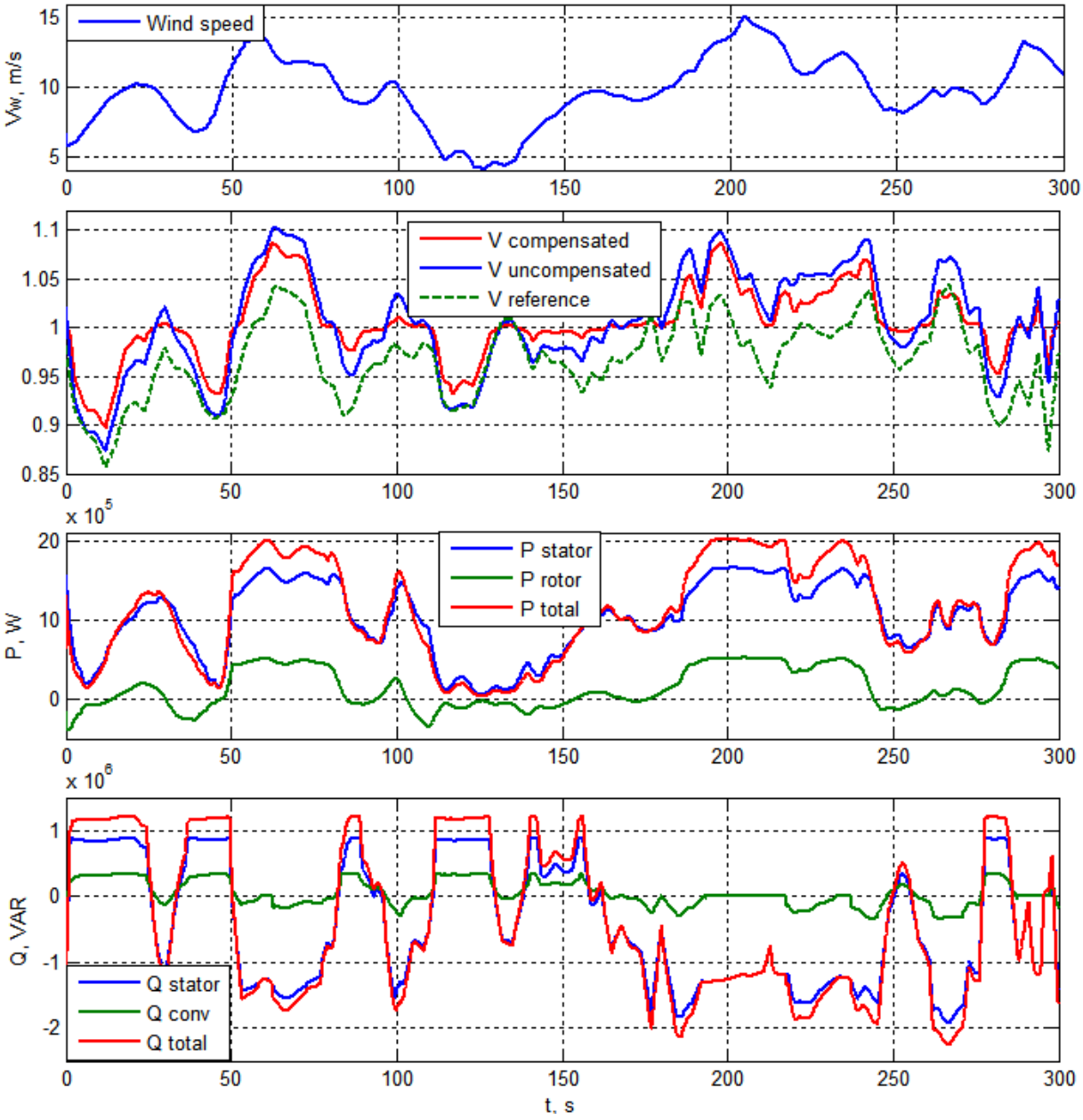

Figure 5.10. Simulation results: Reactive power capabilities of GSC.

6 Conclusions and future work

6.1 Summary

A detailed model of the single DFIG WT system implemented in PLECS simulation environment was taken as a basis for study and modified to be suitable for variable-speed operation at different wind speeds. The model include simulation of such processes as:

- Aerodynamic conversion based on input wind speed considering blades pitch angle control.
- Mechanical conversion process in the drivetrain based on six-mass mechanical model of the drivetrain.
- Detailed power circuit with the DFIG, PWM-fed power converter, LCL-filter and connection to the grid via three-windings transformer and long cable line.

For proper simulation, the vector control system is described and all necessary equations are presented in the time domain for:

- RSC controller references:
    - Calculated torque
    - Active and reactive currents and voltages
    - Stator flux estimation
- GSC controller references:
    - PLL
    - Active and reactive currents and voltages
- WT controller references:
    - Rotor speed for RSC
    - Reactive power for RSC and GSC based on reference value or voltage stabilization algorithm
    - Blades pitch angle

Based on developed model, there was implemented a set of simulations to investigate behavior and controllability of the DFIG WT system in different grid conditions and wind speeds. The set of simulation confirms the data found in other related studies.

Firstly, the power distribution across the circuits in steady-state operation was investigated. Steady-states were considered in dynamic model with high time of simulations, which allows to consider absence of noticeable transitions. The power distribution analysis confirms next statements:

- Power rating of the RSC determines the possible slip values of the DFIG and therefore variable-speed operating range.
- Operation of the RSC is limited at low wind speeds by the rotor voltage rating, while at high wind speeds both rotor voltage and rotor current ratings define the power limitation.
- The most intense operation of the RSC has been observed at high wind speeds, hence RSC power rating should be set according to the maximum rotor speed operation (the highest negative slip value).

The behavior of the DFIG WT was investigated at the low wind speeds and high wind speeds. The simulation allowed to indicate that below the lowest operating wind speed, the DFIG goes to motoring mode as rotor speed goes below minimum stator flux angular speed developed by the RSC and defined by the RSC voltage rating, so in such situation DFIG should be disconnected from the grid.

Provided set of simulations illustrated the principles of DFIG WT operation, such as:

- Distribution of power flows in stator and rotor circuits;
- Pitch angle control;
- Interconnection of power converter current and voltage limitations and WT power rating.

Investigation and implementation of the DFIG WT performance allowed to obtain a model, which is suitable for investigation of dynamic processes in time-based wind speed variations.

Then the reactive power capabilities of DFIG WT was studied. It was indicated, that in pure active operation DFIG WT still requires reactive power flow in rotor circuit and stator constantly absorbs reactive power from the grid for magnetization. After that reactive power capabilities of DFIG WT rated for pure active operation are indicated at variable-speed operating range. It is shown, that while WT rated only for active generation cannot be a source of reactive power at rated wind speeds and above, at lower wind speeds it has a reactive power control capabilities, as RSC currents are far below the limitation.

In previous chapter, the reactive power capabilities of the DFIG WT were investigated. It is shown that for normal operation DFIG requires reactive power flow in rotor circuit. It is also indicated that reactive power is also constantly absorbed by the stator to produce magnetizing flux.

Then reactive power capabilities of the DFIG WT rated for only active power generation are investigated and Q(Wind speed) diagram are plotted for both capacitive and inductive operation. According to results, DFIG WT has a great capability to control reactive power at low wind speeds, because of being not fully loaded with current, while at rated wind speeds and above it cannot provide any reactive power control as it runs out of current limitation of the RSC.

Fingrid requirements claim the necessary power factor provided by WTs in both overvoltage and undervoltage conditions. DFIG WT reactive power capabilities therefore investigated at different voltage levels, and it is shown that overvoltage enhances reactive power capabilities, while undervoltage reduces it. It was also indicated, that achieving capacitive power factor requires more reactive current, than providing inductive one. That is explained by initially inductive operation of IG. Therefore, RSC reactive current rating is developed for providing capacitive 0.995 power factor in 90% voltage level to fulfill Fingrid requirements.

As GSC has similar current load as RSC, its reactive power capabilities were investigated in the same manner and total reactive power capabilities of DFIG WT were plotted as Q(Vw) diagram.

As it is very undesirably for WTs to be disconnected from the grid as they require some time to continue normal operation, there is a special voltage sag waveform, that any WT should survive without disconnection. Simulation of DFIG WT behavior during such voltage sag was performed and indicated ability of developed DFIG WT model to handle such faults. However, it is also indicated the disadvantage of the DFIG topology during such faults: as its stator is connected directly to the grid, there is no ability to control machine during deep voltage sags, because magnetic flux drops to zero.

Based on the reactive power capabilities, the grid voltage controller, which only utilizes free current of RSC and GSC (current that is not involved in active power generation) was developed and tested in simulation of grid voltage variations. Results of simulation show that properly designed WT can be used as reactive power compensator with high dynamics.

6.2 Future work

Presented study has indicated several issues and further directions of research.

1. During the study, the model was developed for single WT, while usually wind power generation is provided by wind farms. Wind farms are more complicated systems and it is essential to investigate electrical processes that take place in wind farms caused by simultaneous work of several WTs. For example, wind distribution across the some landscape will lead to different power outputs from different wind turbines that might affect grid power quality. The other important issue is reactive power distribution during compensation effects.
2. While DFIG WT has many advantages, it also has disadvantages in comparison with full-rated topology. Some of them are: problems with the DFIG WT control during voltage sag and slip rings that require expensive maintenance. The modelling and comparison of the DFIG WT and its closest competitor PMSM topology could help to determine, which solution suits the best for particular industrial case.
3. Study has indicated that DFIG WT can be used for reactive power compensation purposes. That raises the issue of determining whether the balance between “redundant”

power rating of the WT to compensate reactive power and whether the need to use separate device, such as STATCOM, to improve grid voltage quality.

References

(n.d.).

Arapogianni, A., & Genachte, A.-B. (2013, January). *Deep water – The next step for offshore wind energy*. The European Energy Association. Retrieved from Deep water: The next step for offshore wind energy: http://decarboni.se/publications/deep-water-next-step-offshore-wind-energy/11-offshore-wind-market-2012

Arnaltes, S. (2003). Comparison of Variable Speed Wind. *International Conference on Renewable Energies and Power Quality*. Vigo (Spain).

Burton, T., Jenkins, N., Sharpe, D., & Bossanyi, E. (2011). *Wind Energy Handbook* (Second ed.). Wiley.

Cartwrigh, L. X. (2006). Direct active and reactive power control of DFIG for wind energy generation. *IEEE Trans. on Energy Conversion*, (pp. 750-758).

Datta, R., & Ranganathan, V. T. (2003). A method of tracking the peak power points for a variable speed wind energy conversion system. *IEEE Trans. Energy Convers., 18*, pp. 163-166.

E. Hendawi, F. K. (2010). Analysis, Simulation and Implementation of Space Vector Pulse Width Modulation Inverter. *International Conference on Application of Electrical Engineering*, (pp. 124-131).

Fingrid's grid code requirements set for wind power plants has been updated. (2015). Retrieved from Fingrid: http://www.fingrid.fi/en/news/announcements/Pages/Fingrid's-grid-code-requirements-set-for-wind-power-plants-has-been-updated.aspx

Fletcher, J., & Yang, J. (2010). Introduction to the Doubly-Fed Induction Generator for Wind Power Applications. In J. Nathwani, *Paths to Sustainable Energy* (p. 676). InTech.

Golestan S, & M, M. (n.d.). Design oriented study of advanced synchronous reference frame phase-locked loops. *IEEE Transactions on Power Electronics. 28*, pp. 765-778. IEEE.

Hoffmann, R. (2002). *A Comparison of Control Concepts for Wind Turbines in Terms of Energy Capture.*

J. Guo, X. C. (2008). Decoupled control of active and reactive power for a grid-connected doubly-fed induction generator. *Third International Conference on Electric Utility Deregulation and Restructuring and Power Technologies*, (pp. 2620-2625).

Kulka, A. (2004). *Pitch and Torque Control of Variable Speed Wind Turbines.* Chalmers University of Technology.

Luo, M. (2013). *Multi-Physical Domain Modeling of a DFIG.* Zurich, Switzerland: Plexim GmbH.

Muyeen, S. M., Tamura, J., & Murata, T. (2009). *Stability Augmentation of a Grid-connected Wind Farm.* London, England: Springer-Verlag London.

Patel, S. (2013, January 12). *IEA: Wind Power Could Supply 18% of World's Power by 2050*. Retrieved from POWER Magazine : Power generation news and jobs in coal, gas, nuclear, renewables: http://www.powermag.com/iea-wind-power-could-supply-18-of-worlds-power-by-2050/

Petersson, A. (2005). *Analysis, modeling and control of doubly-fed induction generators for wind turbines.* Chalmers University of Technology.

Petersson, A., Harnefors, L., & Thiringer, T. (2004). Comparison between stator-flux and grid-flux-oriented rotor current control of doubly-fed induction generators. *Power Electronics Specialists Conference. 1*, pp. 482 - 486. IEEE.

PVV, R. a. (2013). SPWM Based Two Level VSI for Microgrid Applications. *International Journal of Emerging Trends in Electrical and Electronics*, *7*, pp. 3-6.

Renewable Energy Directive. (2012, December 17). Retrieved from Official website of the European Commission: http://ec.europa.eu/clima/policies/transport/fuel/docs/com_2012_595_en.pdf

Reznik, A., Simoes, M., Al-Durra, A., & Muyeen, S. (2014). LCL Filter Design and Performance Analysis for Grid Interconnected Systems. *IEEE Trans. Ind. Appl., 50*, pp. 1225-1232.

S. Muller, M. D. (2002). Doubly Fed Induction Generator Systems for Wind Turbines. *IEEE Industry Applications Magazine*, 26-33.

VTT. (n.d.). Retrieved from Wind energy statistics in Finland: http://www.vttresearch.com/services/low-carbon-energy/wind-energy/wind-energy-statistics-in-finland

Wang, Q., & Chang, L. (2004). An intelligent maximum power extraction algorithm for inverter-based variable speed wind turbine systems. *IEEE Trans. Power Electron.*, *19*, pp. 1242-1248.

Xu, X., De Doncker, R., & Novotny, D. (1988). A stator flux oriented induction machine drive. *Power Electronics Specialists Conference. 2*, pp. 870-876. Kyoto, Japan: IEEE.